On the Efficiency and Accuracy of Simulation Methods for Optimal Power System Operation

Convex Optimization Models for Power System Analysis, Optimal Utilization of VSC-type DC Wind Farm Grids and FACTS Devices

MOHAMADREZA BARADAR

Doctoral Thesis
Stockholm, Sweden 2015

TRITA-EE 2015:022
ISSN 1653-5146
ISBN 978-91-7595-573-5

KTH School of Electrical Engineering
SE-100 44 Stockholm
SWEDEN

Akademisk avhandling som med tillstånd av Kungl Tekniska högskolan framlägges till offentlig granskning för avläggande av teknologie doktorsexamen i elektriska energisystem tisdagen den 9 juni 2015 klockan 10.00 i H1, Teknikringen 33, Kungl Tekniska högskolan, Stockholm.

© Mohamadreza Baradar, June 2015

Tryck: Universitetsservice US AB

Abstract

Recently, significant changes in electric power systems such as rapid development of smart grid and electricity market and integration of non-dispatchable sources have added more complexity to the Power Flow Scheduling (PFS) and Power Balancing (PB) models. For instance, non-dispatchable sources introduce an increasing level of uncertainty in the electricity market and power system operation. One of the solutions for handling these uncertainties in the power system operation is the improvement of system flexibility through a more efficient operation of power systems. On the other hand, efficient operation can be achieved by well capturing variable behavior of uncertain sources such as wind power sources which in turn demands efficient and robust PFS/PB models. This way, a more flexible system, capable of efficiently accommodating higher levels of wind power changes, can be achieved. All these factors increase a need for PFS/PB models such as Power Flow (PF) and Optimal Power Flow (OPF) models which can address these new challenges in an efficient, reliable, and economic way while supporting the power system operation and control. In this regard, various solution methods have been developed for solving different forms of PF/OPF formulation. The difficulty of solving OPF problems increases significantly with increasing network size and complexity. One of these complexities is how to model advanced controllable devices such as HVDC grids and Flexible AC Transmission Systems (FACTS) devices. Accurate handling of these complexities has limited the use of OPF in many real-world applications mainly because of its associated computational challenges. The main reasons behind computational challenges are nonlinearity and especially non-convexity of constraints representing power system and its components. In this regard, OPF problems are classified into two main groups. In the first group, researchers adopt Nonlinear programming (NLP) approach to fully represent the nonlinearity of the power system for the sake of accuracy but with the cost of complexity in the model. Computational and theoretical challenges associated with NLP approaches are then used as a motivation towards developing a more simplified OPF model, leading to the second group of OPF models known as Linear Programming (LP) based OPF models. LP approaches are fast, reliable, and especially convex, and therefore guarantee a global optimum to the simplified OPF problem. The problem of LP approach to OPF is that the LP solution of OPF

may not even be a feasible solution of original nonlinear OPF at all. Another issue associated with LP models is that complex power system devices such as HVDC links are difficult to be incorporated. These limitations have restricted the application of LP approaches for many OPF problems. According to the mentioned advantages and disadvantages of NLP and LP based OPF models, what we seeks is an OPF model which can have main advantages of both LP OPF models (Efficient numerical solvers) and full AC OPF models (Results accuracy). In this thesis, we develop convex optimization problems which can be adopted as both PF and OPF models which are capable of catching the nonlinear nature of power systems as much as possible while can be solved by efficient solution methods such as Interior Point Methods (IPMs). These OPF models can incorporate HVDC links, wind farm Multi Terminal HVDC (MTDC) grids, and shunt FACTS devices.

Acknowledgment

First of all I would like to appreciate ELEKTRA for the financial support of this project.

I would like to thank Professor Lennart Söder, head of the department of Electric Power Systems (EPS), for providing me and my colleagues with an excellent academic environment.

I wish to express my sincere gratitude to my main supervisor, Associate Professor Mohammad Reza Hesamzadeh, for his continual patience, encouragement and guidance he has so far provided me with. He well taught me how to formulate the problems that I have faced in order to solve them in a more efficient way. I also thank him for reading and reviewing my papers and this thesis and giving me a bunch of useful feedbacks and comments.

I would like to thank my second supervisor Professor Mehrdad Ghandhari for his useful feedbacks and supervision during this project especially in the first two years of my project.

I would also like to thank Assistant Professor Dirk Van Hertem at KU LEUVEN, my former co-supervisor in the first year of this project, for fruitful and efficient meetings we had.

I wish to thank my steering group meeting's members, Kerstin Linden, Magnus Callavik and Inger Segerqvist from ABB, Magnus Danielsson from Svenska Kraftnät and Jonas Persson from Vattenfall for their valuable and technical feedbacks to my project during the meetings and discussions we have had.

I extend my personal thanks to all my colleagues at EPS and other departments for creating an enjoyable studying atmosphere.

I am most grateful to my siblings especially my older brother who has been always helping me how to optimize my life which has been subjected to a highly non-linear set of constraints.

Lastly, my endless gratitude to my parents, my first coaches and mentors. All their supports and love have been the greatest gift to me over these years.

Contents

List of Figures

List of Tables

Abbreviations

PFS	Power Flow Scheduling
PB	Power Balancing
PF	Power Flow
OPF	Optimal Power Flow
NLP	Nonlinear Programming
LP	Linear Programming
HVDC	High Voltage Direct Current
MTDC	Multi-Terminal HVDC
FACTS	Flexible AC Transmission Systems
DC-PF	DC Power Flow
SLP	Sequential Linear Programming
QP	Quadratic Programming
CAC-OPF	Conic AC Optimal Power Flow
CAD-OPF	Conic AC-DC Optimal Power Flow
IPM	Interior Point Method
CPF	Conic Power Flow
ECPF	Extended Conic Power Flow
LMP	Locational Marginal Price
VSCCAD-OPF	Voltage Stability Constrained CAD-OPF
VSM	Voltage Stability Margin
VSC	Voltage Source Converter
SOCP	Second Order Cone Programming
QCP	Quadratically Constrained Problem
STPF	Standard Power Flow
SDP	Semidefinite Programming
EEX	European Energy Exchange
QCQP	Quadratically-Constrained Quadratic Program
FAC-OPF	Full AC Optimal Power Flow
NR	Newton-Raphson
STATCOM	Static Synchronous Compensator
SVC	Static VAR Compensator
FSWT	Fixed-Speed Wind Turbine
DFIG	Doubly Fed Induction Generators
SRSM	Stochastic Response Surface Method
PDF	Probability Density Function
WF	Wind Farm

Part I

Background and Introductory Part

Chapter 1

Introduction

1.1 Background

Recently, significant changes in electric power systems have brought many challenges to traditional AC power systems. Rapid developments in smart grid and electricity market, increasing penetration level of non-dispatchable wind and solar powers to the existing AC power system, [5,6], and power system interconnections have added more complexity especially to the Power Flow Scheduling (PFS) and Power Balancing (PB) analytical models. For instance, wind power integration introduces an increasing level of uncertainty in electricity market and power system operation problems.

The wind power uncertainty can be properly handled by improving the performance of stochastic models and improving the system flexibility by efficient operation of power systems, [7]. The system flexibility improvement through efficient system operation can be achieved by capturing variable behaviour of wind power which in turn demands efficient and robust PFS/PB models to handle wind power changes in shorter time scales. This results in having a more flexible system which is capable of efficiently accommodating wind power changes. All these factors increase a need for more reliable and efficient PFS/PB models such as Power Flow (PF) and Optimal Power Flow (OPF) which can address these new challenges in an efficient, reliable, and economic way while supporting the power system operation and control. This in turn demands an efficient PF/OPF model where the non-linear nature of power system can be modeled in a more accurate way. The PF/OPF models have been widely used in different aspects of steady state analysis such as power system operation, analysis, and planning, [8].

The OPF, firstly introduced by Carpentier in 1962 [9], has been widely used as a tool to optimize a variety of objectives through optimally dispatching power flow within a network subjected to technical limits. The OPF involves multiple PF problems which are iteratively solved in order to maximize/minimize a given objective. Due to nonlinear and non-convex nature of power flow equations, the general

OPF problem is a nonlinear, non-convex optimization problem, [10]. Various solution methods have been developed for solving different forms of OPF formulation. Almost in all of them it has been attempted to develop a software which is capable of solving OPF problems reliably, [11]. The difficulty associated with solving OPF problems increases significantly with increasing network size and complexity. This complexity becomes even more serious for AC systems with embedded advanced controllable devices, namely, Multi-Terminal HVDC (MTDC) grids and Flexible AC Transmission Systems (FACTS) devices.

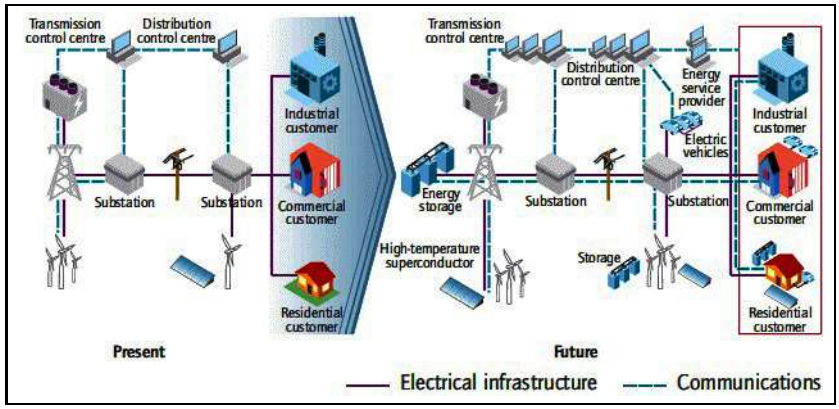

Figure 1.1: Future and present smart grid infrastructure and increasing wind power penetration , [1].

These challenges have limited the use of OPF in many real-world applications, [12,13]. There is a wide variety of OPF formulations and optimization methods in the literature to address these challenges, [14–20].

As a summary of the relevant literature, the more accuracy is needed to represent power systems, the more computational challenges are expected while solving the OPF problem. The main reasons behind these computational challenges stem from nonlinearity and especially non-convexity of AC power flow equations and constraints associated with advanced controllable devices, [21]. In this regard, OPF problems are classified into two main groups. In the first group, researchers adopt Nonlinear Programming (NLP) approach to fully represent the nonlinearity of the power system for the sake of accuracy but with the cost of complexity in the model. Through some of these NLP formulations, it has been tried to reduce the degree of nonlinearity by reformulating the OPF problem through different sets of variables to improve computational aspects of the problem, [18, 19, 22].

The computational and theoretical challenges associated with NLP approaches are then used as a motivation towards developing a more simplified OPF formulation using Linear Programming (LP) approach. Using LP approaches, the nonlin-

earity and non-convexity of the full AC-OPF model were completely removed from the problem. This made it possible to solve the OPF problem using well-developed LP solution methods, such as Simplex Method. Through these methods it is possible to efficiently handle inequality constraints and quickly recognize problem infeasibility. They are fast, reliable, and especially convex, and therefore guarantee a global optimal solution to the simplified OPF problem. It should be noted that the obtained global optima are not the global optima to the original nonlinear AC-OPF. The LP formulations can be obtained through both simplifying assumptions and linearization.

A well-known application of LP formulation to the AC-OPF problem is the use of linear DC Power Flow (DC-PF) equations obtained using simplifying assumptions with a linear objective function, [23]. The DC-OPF is not iterative and outputs the optimal solution through a single solution. Because of its simplicity, speed, and robustness, DC-OPF is widely used, [12]. In addition to the simplified assumptions used in DC-OPF models, one can linearize power flow equations around the current operating point, [11, 24]. This technique is mostly used in the algorithms based on Sequential Linear Programming (SLP).

All these LP approaches are well-suited for the cases where there are convex objective functions. However, for those problems with non-separable objective function such as transmission loss minimization, LP based OPFs are not effective resulting in a significant inaccuracy, [25]. Beside these, the solution of LP based OPF may not even be a feasible solution of original nonlinear OPF at all. The LP problem's global optimal solution is not guaranteed to be the original NLP problem's global optimum. It may not even be a feasible solution at all. Another issue associated with LP based OPF models is that complex power system devices such as HVDC links, which can bring many benefits such as flexibility and a better integration of renewable energies to conventional power systems, are difficult to be modeled. These limitations have restricted the application of LP approaches for many OPF problems, [26].

As an alternative to LP approaches, Quadratic Programming (QP) approach which is a special form of NLP with a quadratic objective function and linear constraints was proposed, [27]. QP-based OPF models were introduced to be used for those cases where LP approaches perform poorly, such as for transmission loss minimization problems. Like LP, the QP requires a local linearization of the power system constraints, and therefore suffers from many of the same accuracy issues. However, QP can directly represent quadratic objective functions, such as generator cost functions. According to mentioned advantages and disadvantages of NLP and LP based OPFs, what we seeks is an OPF model which can have the main advantages of both LP based OPF models (Efficient numerical solvers) and full AC OPF models (Results accuracy). In other words, the desire is to develop a convex OPF model to be capable of catching the nonlinear nature of power systems as much as possible while can be solved efficiently. This OPF model should be also able to incorporate HVDC-grids and FACTS devices. The next section presents steps that we take to achieve this goal.

1.2 Scope and aim of thesis

First of all, the aim of this thesis is to develop PF and OPF models which can have main advantages of both approximated models (Efficiency) and full AC models (Accuracy). In other words, the desire is to develop solution models which are capable of capturing as much nonlinearity as possible of power systems while can be solved efficiently. Secondly, these models should incorporate advanced controllable devices such as HVDC-grids and FACTS device.

To this end, firstly, we reformulate the nonlinear conventional Power Flow (PF) equations using a new set of variables based on line flows for radial networks. State variables in the proposed model consist of bus voltages, active and reactive power flows and losses of lines which reflect more practical knowledge of the system. Having done this, the PF problem is represented as a convex optimization problem in the form of conic programming. This is done by a convex relaxation which is shown that it is exact at the optimality. Through the proposed convex relaxation, the AC power flow problem is recast as a conic optimization problem which is a general form of linear programming with some additional nonlinear constraints in the form of convex cones.

The model is then extended to incorporate constraints associated with existing loops in AC meshed networks through a good approximation. Both efficiency and accuracy of the proposed models are discussed. Afterwards, the model is extended to a Conic AC-DC OPF (CAD-OPF) model for AC power systems incorporating VSC-DC grids and shunt FACTS devices. All proposed optimization models are convex and therefore can be efficiently solved through Interior Point Methods (IPMs). Finally, we develop the CAD-OPF to study the impact of wind power integration on voltage stability margin. We propose a model where system operator is able to ensure a certain voltage stability margin while the wind power penetration level into the grid is maximized.

1.3 Contribution of Thesis

This thesis addresses different steady state aspects of radial and meshed AC systems together with hybrid AC-DC systems incorporating HVDC and shunt FACTS devices without and with wind power penetration.

The contributions of the thesis are listed as follows:

- As the first contribution, a convex optimization problem is proposed as a solution tool for AC power flow problems leading to more robustness and efficiency. The proposed Conic PF (CPF) model is achieved for radial networks through reformulation of conventional AC power flow equations and applying an exact relaxation to render the problem convex. State variables in the proposed optimization problem consist of bus voltages, active and reactive

power flows and losses of lines which reflect more practical knowledge of the system. The obtained set of equations is then used as a set of constraints in an optimization problem where the choice of objective function makes the proposed relaxation exact. The proposed optimization problem is exactly in the form of conic optimization problem which is a convex model and can be efficiently solved through Interior Point Methods (IPMs). The proposed conic optimization problem can efficiently and robustly handle both well- and ill-conditioned radial networks.

- As the second contribution, this thesis proposes a good approximation to extend proposed CPF for meshed AC PF problems. Using proposed approximation and graph theory, nonlinear set of equations associated with phase angle constraints becomes linear and therefore well-suited to be incorporated into the CPF model. The Extended CPF (ECPF) can efficiently and robustly handle both well- and ill-conditioned meshed networks. Although the approximation used in the ECPF model affects the accuracy of results, the output of ECPF model is very close to results from other approaches.
- As the third contribution, the proposed ECPF model is extended to an AC-OPF model where the objective is to minimize generation costs. Since the quadratic generation cost function is not consistent with the conic format, we propose a conic format of quadratic cost function. The proposed Conic AC-OPF (CAC-OPF) model is a convex problem with a good accuracy. According to literature and numerical results in this thesis, the relaxed inequalities used in the proposed CAC-OPF are always binding at the optimality provided that the objective functions is convex and positive and Locational Marginal Prices (LMPs) at all system buses are positive.
- As the forth contribution, a penalized version of CAC-OPF is proposed to handle negative LMPs, if any. The miscalculation of negative LMPs has been reported to be a problem in conic based OPFs.
- As the fifth contribution, a Conic AC-DC OPF (CAD-OPF) model is proposed for AC power systems incorporating VSC-DC grids and shunt FACTS devices. It is shown that the objective function can be optimized through optimal tuning for settings of these controllable devices.
- Finally, as the seventh contribution, a Voltage Stability Constrained CAD-OPF (VSCCAD-OPF) is developed. This proposed VSCCAD-OPF model is to analyze one of the challenges the power systems experience as a result of intermittent nature of wind power outputs. The VSCCAD-OPF model can be adopted by power system operators in order to ensure a certain Voltage Stability Margin (VSM) for wind power integration. The objective of the proposed optimization model is to maximize the wind power penetration level from available realized wind power while ensuring a certain VSM by optimal tuning of installed VSC-HVDC links connecting wind farms to the grid.

1.4 List of Publications

Letters

- **Paper 1**: **Baradar, M.**; Hesamzadeh, M.R., "AC Power Flow Representation in Conic Format," *Power Engineering Letter, Power Systems, IEEE Transactions on* , vol.30, no.1, pp.546,547, Jan. 2015.

Journal Papers

- **Paper 2**: **Baradar, M.**; Ghandhari, M., "A Multi-Option Unified Power Flow Approach for Hybrid AC/DC Grids Incorporating Multi-Terminal VSC-HVDC," *Power Systems, IEEE Transactions on* , vol.28, no.3, pp. 2376, 2383, Aug. 2013.
- **Paper 3**: **Baradar, M.**; Hesamzadeh, M.R.; Ghandhari, M., "Second-Order Cone Programming for Optimal Power Flow in VSC-Type AC-DC Grids," *Power Systems, IEEE Transactions on* , vol.28, no.4, pp.4282,4291, Nov. 2013.

Conference Papers

- **Paper 4**: **Baradar, M.**; Ghandhari, M.; Van Hertem, D., "The modeling multi-terminal VSC-HVDC in power flow calculation using unified methodology," *Innovative Smart Grid Technologies (ISGT Europe), 2011 2nd IEEE PES International Conference and Exhibition on* , vol., no., pp.1,6, 5-7 Dec. 2011.
- **Paper 5**: **Baradar, M.**; Ghandhari, M.; Van Hertem, D.; Kargarian, A., "Power flow calculation of hybrid AC/DC power systems," *Power and Energy Society General Meeting, 2012 IEEE* , vol., no., pp.1,6, 22-26 July 2012.
- **Paper 6**: **Baradar, M.**; Hesamzadeh, M.R.; Ghandhari, M., "Modelling of multi-terminal HVDC systems in optimal power flow formulation," *Electrical Power and Energy Conference (EPEC), 2012 IEEE* , vol., no., pp.170,175, 10-12 Oct. 2012.
- **Paper 7**: **Baradar, M.**; Hesamzadeh, M.R.; Ghandhari, M., "Ohmic loss minimization in AC transmission systems with embedded DC grids," *Industrial Electronics Society, IECON 2013 - 39th Annual Conference of the IEEE* , vol., no., pp.2117, 2120, 10-13 Nov. 2013
- **Paper 8**: **Baradar, M.**; Hesamzadeh, M.R., "Calculating negative LMPs from SOCP-OPF," *Energy Conference (ENERGYCON), 2014 IEEE International* , vol., no., pp.1461,1466, 13-16 May 2014

- **Paper 9**: **Baradar, M.**; Hesamzadeh, M.R., "A stochastic SOCP optimal power flow with wind power uncertainty," *Power and Energy Society General Meeting, 2014 IEEE* , vol., no., pp.1,5, 27-31 July 2014.

Additional Publications

- **Paper 10**: Kargarian, A.; Falahati, B.; Yong Fu; **Baradar, M.**, "Multiobjective optimal power flow algorithm to enhance multi-microgrids performance incorporating IPFC," *Power and Energy Society General Meeting, 2012 IEEE* , vol., no., pp.1,6, 22-26 July 2012.

- **Paper 11**: Nazari, M.; **Baradar, M.**; Hesamzadeh, M.R.; Ghandhari, M., "Online OPF-based Multi-agent Control of Multi-Terminal HVDC Systems Connected to Offshore Wind Farms" accepted for publication in *PowerTech (POWERTECH), 2015 IEEE*, June 2015.

Submitted/to be Submitted Journal Papers

- **Paper 12**: **Baradar, M.**; Hesamzadeh, M. R, " A SOCP Approach for Optimal Tuning of Shunt FACTS Devices and VSC-MTDC Systems", submitted to *International Journal of Electrical Power & Energy Systems*, 2014.

- **Paper 13**: **Baradar, M.**; Hesamzadeh, M. R, "Maximizing Wind Power Penetration Ensuring Voltage Stability Margin", to be submitted to *Electric Power System Research*.

- **Paper 14**: **Baradar, M.**; Hesamzadeh, M. R, "Exercise of Market Power on Ramp-Rate Caused by Wind Power Uncertainties: Analysis and Prediction", to be submitted to *Electric Power System Research*.

1.5 Outline of Thesis

This thesis is presented as follows:

- In chapter 2, a convexified Power Flow Model for radial AC networks is developed and presented. To solve the AC power flow problem, a conic optimization problem which is convex and can be efficiently solved using the Interior Point Methods (IPM) is proposed. The proposed method can reliably and robustly handle the ill-conditioned distribution networks.
- Chapter 3 extends the proposed CPF in chapter 2 to be used for AC power flow calculation of meshed AC networks. The Extended CPF (ECPF) is obtained by reformulating AC power flow equations through three techniques: variable changing, relaxation and approximation. The proposed model can be placed between DC-PF and AC-PF in terms of efficiency and accuracy. The approximations used to derive the ECPF are two well-known approximations used in derivation of DC load flow models.
- Chapter 4 proposes a Conic AC OPF (CAC-OPF) model and the issue of emerging negative Locational Marginal Prices (LMPs) in the proposed conic optimization approach. We show that the negative LMPs, which might be miscalculated through semidefinite problems, can be correctly emerged in the output of proposed CAC-OPF model.
- In chapter 5, followed by chapter 4 the proposed conic format of power flow equations is used to develop a Conic AC-DC OPF (CAD-OPF) model which can be used for hybrid AC-DC grids incorporating VSC-DC grids and shunt FACTS devices. In this chapter, first the equations associated with these devices are derived and then transformed into the perviously proposed conic format.
- Chapter 6 addresses one of the challenges which power systems experience as a result of intermittent nature of wind power output. This is done by modifying perviously proposed CAD-OPF model to ensure a certain voltage stability margin for wind power realization in the real-time operation.
- Finally, in chapter 7 conclusions are presented.

Part II

AC Network Analysis

Chapter 2

Conic Optimization Approach for Power Flow Analysis of Radial Networks

2.1 Introduction

This chapter presents a conic-based approach for AC power flow calculation of radial power systems. The model is convex and can be efficiently solved using Interior Point Methods (IPMs). State variables in the proposed optimization problem consist of bus voltage magnitudes, active and reactive power flows and losses of lines which reflect more practical knowledge of the system. The proposed method can reliably and robustly handle ill-conditioned distribution networks.

2.2 Background

The power flow calculation is a fundamental tool widely used in the steady state analysis of power systems. The standard load flow methods such as Newton-Raphson and fast decoupled methods have a good convergence rate for solving power flow problem of meshed networks. However, these methods have convergence problem in radial networks mostly due to high R/X ratio in the radial networks, [28, 29].

Several solution methods such as backward/forward iterative techniques have been developed to handle this convergence problem, [30, 31]. However, these approaches are relatively time-demanding, [32]. Reference [33] has developed a direct solution method for radial network load flow calculation. In this chapter, we

propose a conic representation for AC power flow calculation of radial networks. Reference [34] has also proposed a Second Order Cone Programming (SOCP) based AC power flow formulation. In this reference, load flow problem is solved through a second order cone optimization problem subject to a set of equations based on the new variable definition. However, unlike reference [34], variables used in our proposed conic format are chosen in such a way to directly output more practical knowledge about the power system. In this thesis, power flow equations are first derived as functions of new variables and then recast as a conic optimization problem. The conic optimization problem is a convex problem which can be efficiently solved using Interior Point Methods (IPM). The proposed model is tested on different case studies including ill-conditioned systems.

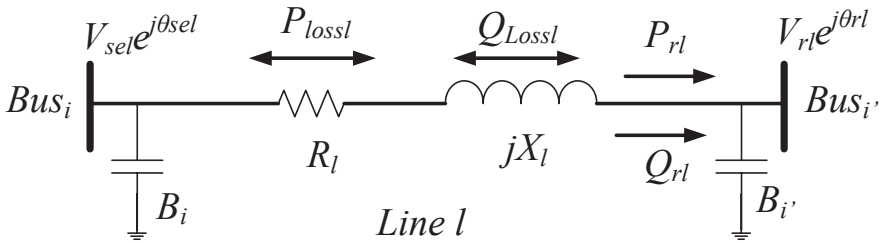

Figure 2.1: The AC line circuit equivalent.

2.3 Derivation of Power Flow Equations

In this section, the line flow equations which are used to fully represent the AC network are derived. Figure 2.1 shows the equivalent circuit of an AC line. Let consider a conventional direction from sending bus indexed by *se* to receiving bus indexed by r for each AC line l (See Figure 2.1). It should be noted that each system bus indexed by i can be either sending or receiving end of an AC line.

According to Figure 2.1, V_i is the voltage magnitude at bus $i \in N_b$ where N_b is the set of AC buses. The V_{sel} and V_{rl} are voltage magnitudes at sending and receiving ends of AC line $l \in N_l$, respectively. The N_l is the set of AC lines. Accordingly, the active and reactive power balance equations for each AC node can be written as follows:

$$P_{gi} - P_{di} = \sum_{l=1}^{n_l} \boldsymbol{M_{PQ}}(i,l) P_{rl} + \sum_{l=1}^{n_l} \boldsymbol{M_{loss}}(i,l) P_{lossl} \tag{2.1}$$

$$Q_{gi} - Q_{di} = \sum_{l=1}^{n_l} \boldsymbol{M_{PQ}}(i,l) Q_{rl} + \sum_{l=1}^{n_l} \boldsymbol{M_{loss}}(i,l) Q_{lossl} - B_i V_i^2 \tag{2.2}$$

where n_l is the number of AC lines. P_{lossl} and Q_{lossl} are active and reactive power losses of each AC line which are obtained as follows:

$$P_{lossl} = \frac{P_{rl}^2 + Q_{rl}^2}{V_{rl}^2} R_l \tag{2.3}$$

$$Q_{lossl} = \frac{P_{rl}^2 + Q_{rl}^2}{V_{rl}^2} X_l \tag{2.4}$$

The elements of incidence matrices $\boldsymbol{M_{PQ}}$ and $\boldsymbol{M_{loss}}$ are determined as follows:

$$\boldsymbol{M_{PQ}}(i,l) = \begin{cases} -1 & \text{if bus } i \text{ is the receiving end of line } l \\ 1 & \text{if bus } i \text{ is the sending end of line } l \\ 0 & \text{if bus } i \text{ is not connected to line } l \end{cases} \tag{2.5}$$

$$\boldsymbol{M_{loss}}(i,l) = \begin{cases} 1 & \text{if bus } i \text{ is the sending end of line } l \\ 0 & \text{otherwise} \end{cases} \tag{2.6}$$

According to Figure 2.1, one can obtain following expression associated with voltage drop across each AC line $l \in N_l$:

$$V_{sel} e^{j\theta_{sel}} = V_{rl} e^{j\theta_{rl}} + \frac{P_{rl} - jQ_{rl}}{V_{rl} e^{-j\theta_{rl}}} (R_l + jX_l) \tag{2.7}$$

If both sides of (2.7) are multiplied by $V_{rl} e^{j\theta_{rl}}$:

$$V_{sel} V_{rl} e^{j(\theta_{sel} - \theta_{rl})} = V_{rl}^2 + (P_{rl} - jQ_{rl})(R_l + jX_l) \tag{2.8}$$

Obtaining the magnitude of both sides in (2.8) and then dividing them by V_{rl}^2:

$$V_{sel}^2 - V_{rl}^2 = 2R_l P_{rl} + 2X_l Q_{rl} + R_l P_{lossl} + X_l Q_{lossl} \tag{2.9}$$

Equation (2.9) is applied to each AC line.

The derived equations representing a radial AC network can be now listed as follows:

$$P_{gi} - P_{di} = \sum_{l=1}^{n_l} \boldsymbol{M_{PQ}}(i,l) P_{rl} + \sum_{l=1}^{n_l} \boldsymbol{M_{loss}}(i,l) P_{lossl} \tag{2.10}$$

$$Q_{gi} - Q_{di} = \sum_{l=1}^{n_l} \boldsymbol{M_{PQ}}(i,l) Q_{rl} + \sum_{l=1}^{n_l} \boldsymbol{M_{loss}}(i,l) Q_{lossl} - B_i V_i^2 \tag{2.11}$$

$$P_{lossl} = \frac{P_{rl}^2 + Q_{rl}^2}{V_{rl}^2} R_l \qquad Q_{lossl} = \frac{P_{rl}^2 + Q_{rl}^2}{V_{rl}^2} X_l \tag{2.12}$$

$$V_{sel}^2 - V_{rl}^2 = 2R_l P_{rl} + 2X_l Q_{rl} + R_l P_{lossl} + X_l Q_{lossl} \tag{2.13}$$

where:
P_{gi} and Q_{gi} are the active and reactive power production of generating units.
P_{di} and Q_{di} are active and reactive power of loads.
P_{rl} and Q_{rl} are active and reactive line flows at receiving end of lines.
P_{lossl} and Q_{lossl} are active and reactive power line losses.

In the set of equations listed in (2.10)-(2.13), constraints (2.10) and (2.11) are associated with AC bus mismatch constraints, constraints (2.12) represent active and reactive power losses of AC line and constraints (2.13) are associated with voltage drop constraints across AC lines.

Assuming substation bus as slack bus, we have a system of equations including $n_e = 2n_b + 3n_l = 5n_b$ equations and $n_x = 5n_l$ variables (in the radial networks $n_b = n_l$ if n_b is the number of buses except for the slack bus). Therefore we have a system of n_e equations with n_x variables where $n_e = n_x$. This means set of equations (2.10)-(2.13) are a full representation of an AC radial network.

2.4 Conic formulation of network constraints

The conic formulation of the network constraints are derived through the following steps:
Change of Variable: We define a new variable $V_i^2 = W_i$ for AC voltage magnitudes to be applied to all equations.
Conic Relaxation: The second step is handling the nonlinear equations associated with transmission losses which makes the feasible region non-convex. First we obtain a linear relation between active and reactive power losses. From (2.3) and (2.4), one can obtain following linear expression:

$$P_{lossl} X_l - Q_{lossl} R_l = 0 \tag{2.14}$$

In order to render the feasible region convex we replace all equalities in the form of (2.3) with the following inequality:

$$P_{lossl} \geq \frac{P_{rl}^2 + Q_{rl}^2}{W_{rl}} R_l \tag{2.15}$$

where W_{rl} is the square of voltage magnitudes at receiving end of AC node of line $l \in N_l$. By defining a new variable $P_{lossl} = 2\beta_{lossl} R_l$, inequality (2.15) can be rewritten as:

$$2\beta_{lossl} W_{rl} \geq P_{rl}^2 + Q_{rl}^2 \tag{2.16}$$

Constraints (2.16) are now in the form of rotated quadratic convex cone, [35].

It will be shown in the following sections that this relaxation is exact. The exactness of proposed relaxation for convexifying transmission loss constraints is also shown through simulation results later in this chapter. However, we will first present the general form of a conic optimization problem.

2.5 Conic Optimization Problem

The conic Optimization Problem (COP) is a convex problem which can be introduced as a general form of LP model accompanied by nonlinear constraints which are in the form of convex cones. Many kinds of problems such as LP, Quadratically Constrained Problems (QCP) can be formulated as COPs and be efficiently solved through polynomial time IPMs, [35,36]. This optimization problem has the following form:

$$\text{Minimize } \mathbf{F^T X} \tag{2.17}$$

$$\text{Subject to } \mathbf{AX} = \mathbf{b} \tag{2.18}$$

$$\underline{\mathbf{X}} \leq \mathbf{X} \leq \overline{\mathbf{X}} \tag{2.19}$$

$$\mathbf{X} \in \kappa \tag{2.20}$$

where $\mathbf{X} \in R^n$ is the optimization variable vector. If the variables are divided into $\mathbf{X} = [\mathbf{Xset_1}^T, ..., \mathbf{Xset_p}^T]^T$ in such a way that each element of $\mathbf{X}$ only belongs to one set of $\mathbf{Xset_m}$, then the additional condition i.e. $\mathbf{X} \in \kappa$ is fulfilled if $\kappa = \{\kappa_1, ..., \kappa_p\}$ is the set of convex cones and:

$$\{\mathbf{X} \in R^n : \mathbf{Xset_m} \in \kappa_m, m = 1, ..., p\} \tag{2.21}$$

Assuming $\mathbf{Xset_m} = [x_1, ..., x_{n_{set_m}}]^T$, each cone κ_m in (2.21) can have two following forms:

Second Order Cone

The standard form of second order cone is as follows:

$$\kappa_{SOC} = \left\{ \mathbf{X} \in R^{n_{set_m}} : x_1 \geq \sqrt{\sum_{k=2}^{n_{set_m}} x_k^2},\ x_1 \geq 0 \right\} \tag{2.22}$$

Rotated Quadratic Cone

This kind of cone is obtained by rotating a κ_{SOC} with an angle of 45 degrees in $x_1 - x_2$ plane which has the following form:

$$\kappa_{RQC} = \left\{ \mathbf{X} \in R^{n_{set_m}} : 2x_1 x_2 \geq \sum_{k=3}^{n_{set_m}} x_k^2,\ x_1, x_2 \geq 0 \right\} \tag{2.23}$$

Therefore if an optimization model with a linear objective function is subjected to a set of linearly independent functions and some convex inequalities with above forms, the problem is a convex conic optimization model. The proposed Conic Power Flow (CPF) problem is now represented as following convex optimization problem:

$$Minimize \sum_{l \in N_l} \beta_{lossl} \tag{2.24}$$

subject to

$$(\forall i \in N_b,\ \forall l \in N_l)$$

$$P_{gi} - P_{di} = \sum_{l=1}^{n_l} \boldsymbol{M_{PQ}}(i,l) P_{rl} + \sum_{l=1}^{n_l} \boldsymbol{M_{loss}}(i,l) P_{lossl} \tag{2.25}$$

$$Q_{gi} - Q_{di} = \sum_{l=1}^{n_l} \boldsymbol{M_{PQ}}(i,l) Q_{rl} + \sum_{l=1}^{n_l} \boldsymbol{M_{loss}}(i,l) Q_{lossl} - B_i W_i \tag{2.26}$$

$$W_{sel} - W_{rl} = 2R_l P_{rl} + 2X_l Q_{rl} + R_l P_{lossl} + X_l Q_{lossl} \tag{2.27}$$

$$X_l P_{lossl} - R_l Q_{lossl} = 0 \tag{2.28}$$

$$P_{lossl} = 2R_l\beta_{lossl} \tag{2.29}$$

$$2\beta_{lossl}W_{rl} \geq P_{rl}^2 + Q_{rl}^2 \tag{2.30}$$

The choice of objective function in this optimization problem allows us to use the relaxation (replacing equality with inequality) in (2.30). The objective function forces the inequalities in (2.30) to become binding at the optimality. The relaxed inequalities in (2.30) are always binding at the optimality provided that there is a feasible solution to the problem and objective function is convex, [37]. This will be numerically studied through the simulation results. The above optimization problem has all characteristics of a convex conic program introduced in (2.20) and can be efficiently solved through polynomial time IPMs, [38].

2.6 Case Study and Simulation Results

To evaluate the proposed CPF model, five test systems from literature are used. The model is coded in commercial software GAMS and solved by its embedded MOSEK interior-point optimizer, [39].

Table 2.1: The CPF results for six test systems.(NMI: number of MOSEK iterations NR:Newton-Raphson)

system	Results w.r.t NR	Execution time(s)	Max. Error for $V(p.u.)$	NMI CPF	NMI [34]
12 Bus	Identical	0.03	0 w.r.t [40]	15	16
15 Bus	Identical	0.02	0 w.r.t [41]	13	15
28 Bus	Identical	0.02	$1e-5$ w.r.t [41]	14	21
33 Bus	Identical	0.05	$1e-5$ w.r.t [42]	16	19
69 Bus	Identical	0.05	0 w.r.t [42]	17	30
85 Bus	Identical	0.06	$1e-5$ w.r.t [41]	16	27

Table 2.1 shows a summary of the results. As compared with reference [34] the number of MOSEK iterations for our proposed model is smaller for all reported cases. The CPF results are compared with outputs of other proposed methods in the literature including Newton-based methods.

It should be reported that, as it was expected, inequality (2.30) has been always binding at the optimality. Since the MOSEK solver can efficiently handle the ill-conditioned networks, our proposed optimization problem in (2.24)-(2.29) can efficiently solve the ill-conditioned radial networks, [34, 38]. For those cases where there is no solution to power flow equations, unlike the Newton based methods

which fail to converge (due to exceeding the maximum permitted number of iterations), the MOSEK interior-point optimizer returns a massage that the problem is infeasible.

This chapter proposes a conic format for AC power flow calculation of radial networks. Firstly, the AC Load Flow constraints are derived as function of more practical variables i.e. line power flows, line losses, and square of voltage magnitudes. Then the derived equations are recast as a convex optimization problem through a change of variable and an exact relaxation. The solution of AC power flow is then obtained through solving the proposed optimization problem. The proposed conic optimization problem is coded in GMAS platform and efficiently solved using its embedded MOSEK Interior-Point optimizer. The method is tested on different ill-conditioned case studies. The power flow solution to all cases are efficiently and accurately achieved. Also, through the comparison between our CPF problem and another proposed conic format in the literature, it is shown that our proposed conic optimization problem converges within a lower number of MOSEK iterations.

Chapter 3

Conic Optimization Approach for Power Flow Analysis of AC Meshed Networks

3.1 Introduction

In this chapter the proposed CPF model in chapter 2 is modified and extended to be applied to meshed AC networks. The Extended CPF (ECPF) model is derived through reformulating AC power flow equations using techniques used in the pervious chapter i.e. variable changing, relaxation and an additional approximation technique. The proposed model can be placed between DC-PF and AC-PF in terms of efficiency and accuracy. The approximations used to derive the ECPF are two well-known approximations used in the derivation of DC load flow models.

3.2 Background

In power engineering, power flow analysis is an underlying tool widely used in steady state analysis of power systems. One of the usage of the power flow analysis is initializing variables in dynamic power system simulations, [43]. This chapter addresses the power flow analysis of AC meshed networks. The first method used for solving the AC power flow was Gauss Seidel. One of the drawbacks of this method is its slow convergence rate, [11]. The next approach is Newton Raphson widely used for power flow calculation of power systems which has a better convergence rate than Gauss Seidel approaches. References [44] and [45] are two comprehensive reviews on several power flow solution techniques such as Gauss Seidel and Newton

Raphson. Other solution methods for power flow problems such as biologically inspired ant colony algorithm and genetic algorithm based methods have been also proposed in [46, 47]. These solution techniques have been used for solving different AC power flow representations. Two well-known AC power flow representations are based on power-mismatch and current-mismatch formulations, [48, 49]. In a recent paper an eigenvalue based formulation for power flow calculation has been proposed, [43]. The model in [43], including active and reactive power, and voltage magnitude equations, is reformulated as a multi-parameter eigenvalue problem. However, the formulation cannot be used for the power flow analysis of systems with more than two buses. Reference [50] has also achieved some improvements to a rectangular form of power flow equations. A second order cone programming format for AC power flow formulation of meshed networks was proposed in [51]. In this work, first conventional power flow equations are reformulated based on new variables and then the problem is solved through an optimization problem. However, inside the main optimization problem there is an iterative loop in order to handle some nonlinear equations associated with voltage phase angle constraints.

In present chapter, we develop a power flow formulation in conic format for power flow solution in AC meshed networks. The model presented in this chapter is an extension of CPF model developed in chapter 2. The Extended CPF (ECPF) model is derived through reformulating AC power flow equations using techniques used in the pervious chapter and an additional approximation technique. The ECPF model is also in the form of conic optimization problem. The accuracy of ECPF is shown with numerical examples through comparing results obtained from ECPF model and a Newton Raphson based power flow model.

The ECPF model has the main advantages of both approximated DC PF and full AC PF models. In the other words, the proposed model can be placed between DC-PF and AC-PF in terms of efficiency and accuracy. It is a convex problem containing a set of linear equations accompanied with convex cones. This convex model can be efficiently solved through IPMs.

3.3 Power Flow Equations

In this section, the complete set of equations used in ECPF model is presented. Using derived equations in chapter 2, the set of power flow equations representing a meshed AC network is derived as follows:

$$P_{gi} - P_{di} = \sum_{l=1}^{n_l} \boldsymbol{M_{PQ}}(i,l) P_{rl} + \sum_{l=1}^{n_l} \boldsymbol{M_{loss}}(i,l) P_{lossl} \tag{3.1}$$

$$Q_{gi} - Q_{di} = \sum_{l=1}^{n_l} \boldsymbol{M_{PQ}}(i,l) Q_{rl} + \sum_{l=1}^{n_l} \boldsymbol{M_{loss}}(i,l) Q_{lossl} - B_i V_i^2 \tag{3.2}$$

$$P_{lossl} = \frac{P_{rl}^2 + Q_{rl}^2}{V_{rl}^2} R_l \tag{3.3}$$

$$Q_{lossl} = \frac{P_{rl}^2 + Q_{rl}^2}{V_{rl}^2} X_l \tag{3.4}$$

$$V_{sel}^2 - V_{rl}^2 = 2R_l P_{rl} + 2X_l Q_{rl} + R_l P_{lossl} + X_l Q_{lossl} \tag{3.5}$$

$$V_{sel} V_{rl} \sin(\theta_{sel} - \theta_{rl}) = X_l P_{rl} - R_l Q_{rl} \tag{3.6}$$

where (3.5) was derived in chapter 2 by obtaining magnitude of both sides of (2.8). Expression (3.6) is derived by setting the imaginary part of left side of (2.8) equal to the imaginary part of right side of (2.8). In (3.6), $\theta_{srl} = \theta_{sel} - \theta_{rl}$ is the difference phase angle between sending and receiving ends of AC lines $l \in N_l$. In the set of equations listed in (3.1)-(3.6), the (3.1) and (3.2) are associated with AC buses' mismatch constraints, (3.3) and (3.4) represent the active and reactive power losses in each AC line, (3.5) is associated with voltage drop across each AC line and constraint (3.6) is associated with the phase angle difference across each AC line. In above equations, there are three sets of non-convex constraints where two of them i.e. (3.3) and (3.4) were convexified through conic relaxation proposed in pervious chapter (i.e. (2.30) and (2.28)). The constraints (3.6) will be handled in this chapter.

Constraints associated with phase angle difference (3.6) have been handled through different techniques in the literature. For AC meshed networks, authors in reference [52] show that if the phase angle constraints are eliminated from the original OPF problem and then a conic relaxation is applied, the resulting problem has an exact solution of the original problem provided that some necessary conditions are met. These conditions include no upper bound on active and reactive loads (load over-satisfaction) and successful angle recovery. They introduced some conditions under which the removed phase angles constraints can be recovered. It is shown that the phase angle recovery conditions are always valid for the tree networks, whereas it fails for the meshed networks in some cases. To handle this problem, they proposed installing a number of phase shifters in the meshed network to satisfy the phase angle recovery conditions. To handle the phase angle constraints, reference [53] eliminates the phase angle constraints from the whole power flow equations and assumes all voltage magnitudes are equal to unity in all equations. In another work, phase angle constraints are approximated by the first-order Taylor Series, [51]. In reference [51], an extra iterative loop is proposed to linearize these phase angle constraints.

In this thesis, we propose a simple approximation technique to render nonlinear constraints associated with phase angle constraints as a linear set. Doing this, the phase angle constraints are well integrated into the proposed conic model without

any external iterative loops. This makes our model as a one-shot optimization problem. We apply two well-known approximations $sin\theta_{sr} \approx \theta_{sr}$ and $V_{sel}V_{rl} \approx 1$ only to constrains (3.6). Doing this, (3.6) can be rewritten as follows:

$$\theta_{sr_l} = X_l P_{rl} - R_l Q_{rl} \tag{3.7}$$

There are other works which formulate different conic PF formulations. In these works, voltage phase angle constraints are linearized using Taylor Series around the operating point resulting in a more accurate solution but with the cost of more complication. For example, proposed formulation in [51] has used an iterative solution method to handle these nonlinear equations. Having applied the approximation technique and obtaining constraints (3.7), the proposed ECPF model for solving AC power flow calculation of AC meshed networks is presented as follows, [54]:

$$Minimize \sum_{l \in N_l} \beta_{lossl} \tag{3.8}$$

$$subject\ to$$

$$(\forall i \in N_b,\ \forall l \in N_l)$$

$$P_{gi} - P_{di} = \sum_{l=1}^{n_l} \boldsymbol{M_{PQ}}(i,l) P_{rl} + \sum_{l=1}^{n_l} \boldsymbol{M_{loss}}(i,l) P_{lossl} \tag{3.9}$$

$$Q_{gi} - Q_{di} = \sum_{l=1}^{n_l} \boldsymbol{M_{PQ}}(i,l) Q_{rl} + \sum_{l=1}^{n_l} \boldsymbol{M_{loss}}(i,l) Q_{lossl} - B_i W_i \tag{3.10}$$

$$W_{sel} - W_{rl} = 2R_l P_{rl} + 2X_l Q_{rl} + R_l P_{lossl} + X_l Q_{lossl} \tag{3.11}$$

$$X_l P_{lossl} - R_l Q_{lossl} = 0 \tag{3.12}$$

$$2\beta_{lossl} W_{rl} \geq P_{rl}^2 + Q_{rl}^2 \tag{3.13}$$

$$\mathbf{C}(lop,l) X_l P_{rl} - \mathbf{C}(lop,l) R_l Q_{rl} = 0 \tag{3.14}$$

Expression (3.13) is in the form of rotated quadratic cone which is a convex cone. Set of equations in (3.14) are derived using graph theory, stating that the phase angle difference around each independent loop in a meshed graph is zero. If n_{lo} is

the number of independent loops and n_l the number of branches in a graph, $\mathbf{C}$ is a matrix whose elements are obtained as follows:

$$\boldsymbol{C}(lo,l) = \begin{cases} 1 & \text{line } l \text{ is in loop } lo \text{ with the same direction} \\ -1 & \text{line } l \text{ is in loop } lo \text{ with the opposite direction} \\ 0 & \text{line } l \text{ is not in loop } lo \end{cases} \tag{3.15}$$

The number of equations is sum of $2n_b$ (from (3.9) and (3.10)), $3n_l$(from (3.11), (3.12) and (3.13)), and $n_l - n_b + 1$ (from (3.14)) equations which equals to $n_e = 4n_l + n_b + 1$. If n_g is the number of generator buses, assuming that there is one slack bus, there are $n_b - n_g$ PQ buses and $n_g - 1$ PV buses. State variables consist of receiving ends' active and reactive power flows and losses for each line ($4n_l$ variables), square of voltage at PQ buses ($n_b - n_g$), active power (one variable) at slack bus and reactive power generation at generator buses (n_g variables). This gives us the number of variables $n_x = 4n_l + n_b + 1$. Therefore we have a system of n_e equations and n_x variables in which $n_e = n_x$. This means set of constraints (3.9)-(3.14) is a full represntnation of a meshed AC network. The above optimization problem has all characteristics of a convex conic optimization problem. It has linear objective function subject to a set of linear constraints accompanied by a nonlinear but convex set of constraints in the form of convex cones. The linear term in the objective function again allows us to use the conic relaxation in (3.13). This term in the objective function forces the inequality in (3.13) to become binding at the optimality.

3.4 Case Study and Simulation Results

To evaluate the proposed ECPF model, first three small test systems including the 4 bus system in [55] (See Figure 3.1), and the IEEE 14 and IEEE 30 test systems in [56] are used as case studies. The results of proposed formulation obtained from MOSEK solver in GAMS are compared with those obtained from an AC Standard PF (STPF) program. The power flow results associated with 4 bus test system are given in Table 3.1.

The results given in Table 3.1 highlights the good accuracy of the proposed ECPF model. Table 3.2 and Figure 3.2 show the results for IEEE 14 bus test system.

A short summary of results for IEEE 30 bus test system is given in Table 3.3. In all tables the execution time and maximum errors for voltage magnitudes and phase angles are given.

To evaluate the application of ECPF model for larger test systems, a summary of results obtained for three larger test systems are reported in Table 3.4. As it is observed from simulation results in this section, small errors indicate very good accuracy of the ECPF model even with the approximation we used in phase angle constraints. It should be highlighted that inequalities (3.13) have been always binding at the optimality in all simulations in this section. One special characteristic of

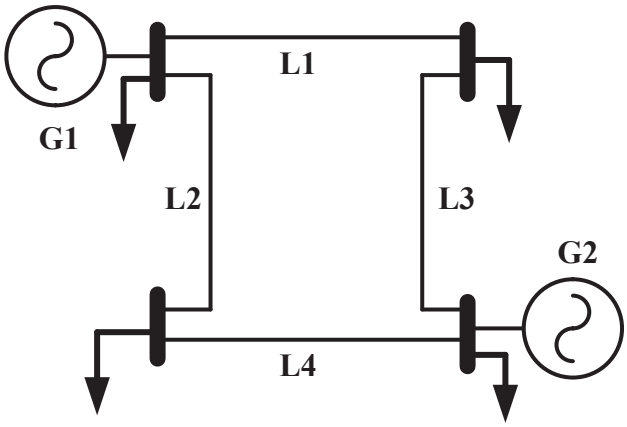

Figure 3.1: The 4-bus example system.

Table 3.1: Power flow results from STPF and ECPF for 4 bus test system.(* indicates slack bus and ** indicates PV buses)

Program	**AC Bus**	**Voltage** ($p.u.$)	**Phase** (deg)	P_{gi} (MW)	Q_{gi} (MW)
STPF	1	1.000*	0	186.81	114.50
ECPF	1	1.000	0	186.83	115.60
STPF	2	0.9820	-0.976	0	0
ECPF	2	0.9818	-0.972	0	0
STPF	3	0.9690	-1.872	0	0
ECPF	3	0.9690	-1.871	0	0
STPF	4	1.0200**	1.523	318.00	181.43
ECPF	4	1.0200	1.522	318.00	182.96
CPF	**Ex.**	**time** (s)	0.03		
STPF-ECPF	**Max.**	**error** V (p.u.)	1.4e-4		
STPF-ECPF	**Max.**	**error** θ_{sr} (rad.)	9.7e-5		

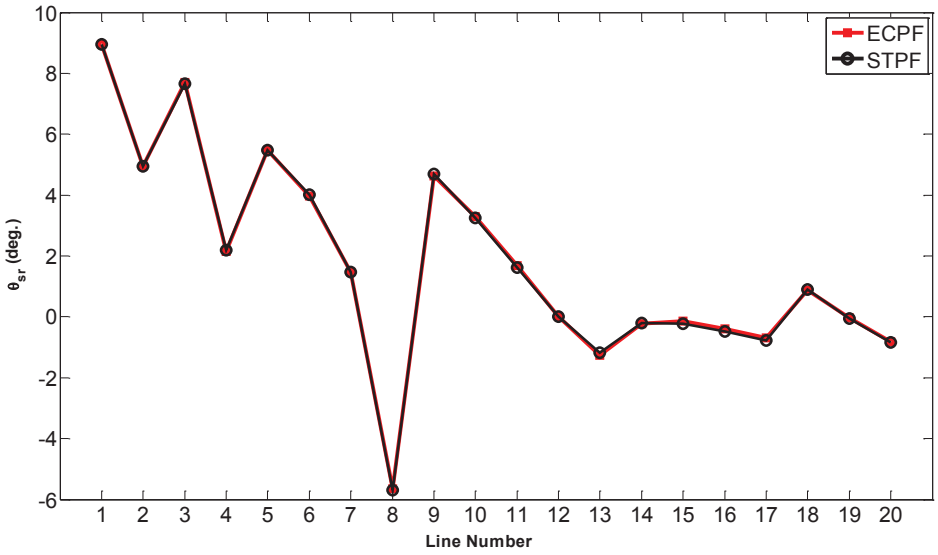

Figure 3.2: Phase angle results from STPF and ECPF models for IEEE 14 bus test system.

the developed ECPF model is that it benefits from MOSEK interior-point solvers, which are well suited for solving ill-conditioned networks, [38, 51]. To show this, a meshed 13-bus ill-conditioned network, which was found difficult to be solved by different methods (See [4]) is tested. Table 3.5 shows a comparison between solutions for this meshed 13-bus ill-conditioned network obtained through our ECPF model and MATPOWER.

Table 3.2: Power flow results from STPF and ECPF for IEEE 14 bus test system. (* indicates slack bus and ** indicates PV buses)

Program	**AC Bus**	**Voltage** ($p.u.$)	P_{gi} (MW)	Q_{gi} ($MVar$)
STPF	1	1.060*	232.42	-23.58
ECPF		1.060	232.42073	-23.64171
STPF	2	1.045**	40.00	27.32
ECPF		1.045	40.00	27.32513
STPF	3	1.010**	-	17.97
ECPF		1.010	-	17.94563
STPF	4	1.023	-	-
ECPF		1.02957	-	-
STPF	5	1.035	-	-
ECPF		1.03509	-	-
STPF	6	1.070**	-	40.58
ECPF		1.070	-	40.72499
STPF	7	1.056	-	-
ECPF		1.05598	-	-
STPF	8	1.090**	-	21.13
ECPF		1.090	-	21.05172
STPF	9	1.049	-	-
ECPF		1.04985	-	-
STPF	10	1.046	-	-
ECPF		1.04601	-	-
STPF	11	1.054	-	-
ECPF		1.05442	-	-
STPF	12	1.055	-	-
ECPF		1.05467	-	-
STPF	13	1.049	-	-
ECPF		1.04955	-	-
STPF	14	1.031	-	-
ECPF		1.03168	-	-
STPF	**Total**	**P-losses**	13.424	
ECPF		(MW)	13.42073	
STPF	**Total**	**Q-losses**	55.45	
ECPF		($MVAR$)	55.45441	
ECPF	**Ex.**	**time** (s)	0.06	
STPF-ECPF	**Max.**	**error** V (p.u.)	$8.5e-4$	
STPF-ECPF	**Max.**	**error** θ_{sr} (rad.)	$2.8e-3$	

Table 3.3: Power flow results from STPF and ECPF for IEEE 30 bus test system.

STPF	**Total**	**P-losses**	18.135
ECPF		(MW)	18.138
STPF	**Total**	**Q-losses**	69.820
ECPF		$(MVAR)$	69.821
STPF	**Total**	**P-Generation**	301.530
ECPF		(MW)	301.538
STPF	**Total**	**Q-Generation**	137.020
ECPF		$(MVar)$	137.026
STPF	**Total**	**Q-Shunt**	59.000
ECPF		$(MVar)$	58.999
STPF-ECPF	**Ex.**	**time** (s)	0.08
STPF-ECPF	**Max.**	**error** V (p.u.)	$7.9e-4$
STPF-ECPF	**Max.**	**error** θ_{sr} (rad.)	$1.2e-3$

Table 3.4: The results of ECPF model for six different example systems. (WCS: well-conditioned system)

WCS	Ex. t. (s)	Max. er. $V(p.u.)$	Max. er. $\theta(rad.)$	NI (ECPF)	NI [51]
57 Bus	0.05	$8.5e-4$	$3.3e-3$	15	60
118 Bus	0.07	$5.3e-4$	$4.1e-3$	12	44
300 Bus	0.09	$9.3e-4$	$8.9e-3$	27	107

Table 3.5: ECPF results for a meshed ill-conditioned test system [4] .(The results are compared to the outputs in MATPOWER. MP: MATPOWER, NI: Number of Iterations, ICS: ill-conditioned system)

ICS	Ex. t. (s)	Max. er. $V(p.u.)$	Max. er. $\theta(rad.)$	NI
13 Bus	0.05 ECPF	$1.15e-2$	$2.85e-2$	13 ECPF
	0.06 MP			4 MP

Chapter 4

Conic AC Optimal Power Flow and Negative Locational Marginal Prices

4.1 Introduction

This chapter proposes a Conic AC OPF (CAC-OPF) model. The issue of miscalculation of negative Locational Marginal Prices (LMPs), if any, through semidefinite OPF models is also studied. Finally, we show that negative LMPs, which might be miscalculated through semidefinite models, can be correctly emerged in the output of proposed CAC-OPF model which is a subset of semidefinite optimization problem.

4.2 Background

The optimal Power Flow (OPF) is a fundamental tool widely used in the power system operation and planning studies. Since OPF was first formulated, several formulations and solution methods for this non-convex and nonlinear problem have been proposed.

Recent research shows that the non-convex OPF problem can be recast as a convex Semidefinite Programming (SDP) problem [57, 58] or conic programming problem, [19,52,53]. This is achieved through eliminating or linearizing constraints associated with phase angle constraints in AC meshed networks together with convex relaxations. Authors in reference [52] show that if phase angle constraints are eliminated from the original AC OPF problem and then a conic relaxation is applied, the resulting problem has an exact solution of the original problem provided

that some conditions are met. These conditions include no upper bound on the active and reactive loads (load over-satisfaction) and a successful angle recovery. They introduced some conditions under which eliminated phase angle constraints can be recovered. It is shown that the phase angle recovery conditions are always valid for radial networks, whereas it fails for meshed networks in some cases. To handle this problem, they proposed installing a number of phase shifters in the meshed network to satisfy the phase angle recovery conditions. To handle phase angle constraints, in other conic formulations, reference [53] eliminates these constraints from the whole power flow equations and assumes all voltage magnitudes to be equal to one in all equations. In reference [19], phase angle constraints are approximated by the first-order Taylor Series. In this reference, an extra iterative loop is proposed to linearize these phase angle constraints.

In this chapter, we propose a Conic AC OPF (CAC-OPF) model where we use conic representation of power flow equations proposed in chapter 3 to form the proposed CAC-OPF model. As described before, through proposed approximations in chapter 3, phase angle constraints can be well integrated into the OPF model through some linear constraints. This way, we avoid the need for an extra iterative loop as proposed in [19].

In the second part of this chapter, we study an issue associated with SDP OPF problems which may lead to miscalculation of negative Locational Marginal Prices (LMPs) as reported in references [3, 59]. This issue stems from emerging a gap between relaxed model and original model. This means the relaxed inequalities might not become binding at the optimality in case there are some negative LMPs in the system.

The negative LMPs (some power consumers in the network are paid to consume more power) are under certain conditions emerged at the optimal solution of an OPF problem. Calculating and monitoring of negative LMPs are important for the electricity market operators and regulators. These are signals of not well-functioning electricity markets and often lead to scrutinizing of the underlaying market design.

The physical interpretation of the negative LMPs is that increasing loads at some system buses can reduce the total generation cost by relieving congestion elsewhere in the network. This allows cheaper generators to output more power and therefore total generation cost to be reduced.

There are few cases where power markets operate with some negative LMPs. As an example, we use the contour map of LMPs throughout MidwestISO system in U.S. which is accessible in [2] (See Figure 4.1). The LMPs are updating every 5-minute. As it is seen in Figure 4.1, there are some periods in summer 2011 where negative LMPs have occurred in the system many times with the most negative price of \$-112 per MWh.

There are also some cases where negative LMPs are as a result of that some generation units offer negative bids in the market auction. The German power

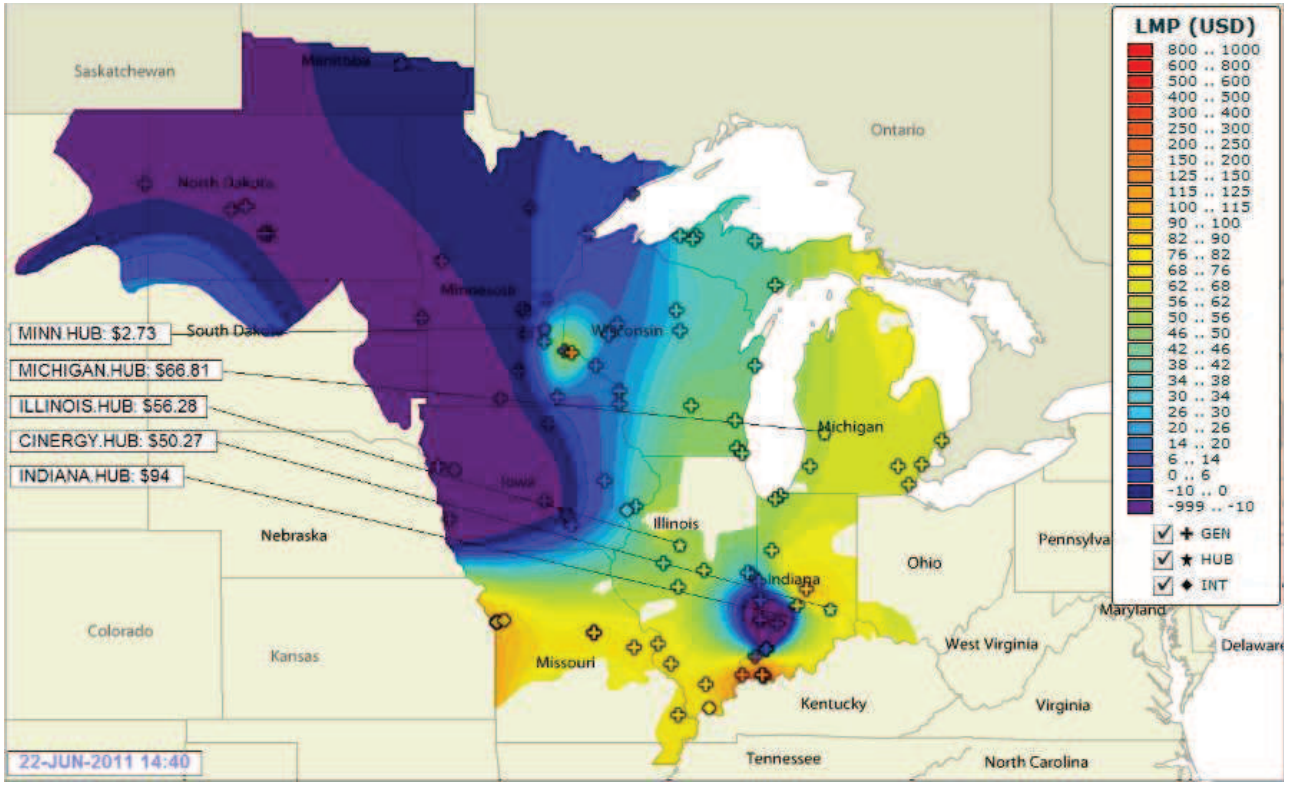

Figure 4.1: Occurrence of Negative LMPs in the MidwestISO Market, [2, 3].

exchange EEX is one of these cases, [60, 61]. Therefore, an OPF model has to be able to correctly calculate negative LMPs, if any.

In this chapter, we address the issue of miscalculation of negative LMPs associated with binding physical constraints such as congestion on transmission lines using our CAC-OPF model. Finally, we show that our proposed OPF model can correctly output negative LMPs by adding a linear term to the objective function of the problem.

4.3 The AC Conic OPF (CAC-OPF) Model

We use the same set of equations derived in chapter 3 as constraints of CAC-OPF. The objective is to minimize generation costs of all generating units as follows:

OPF1:

$$Minimise \sum_{g \in N_g} QCF_g(P_g) \tag{4.1}$$

$$subject\ to$$

$$(\forall i \in N_b,\ \forall l \in N_l)$$

$$P_{gi} - P_{di} = \sum_{l=1}^{n_l} \boldsymbol{M_{PQ}}(i,l) P_{rl} + \sum_{l=1}^{n_l} \boldsymbol{M_{loss}}(i,l) P_{lossl} \tag{4.2}$$

$$Q_{gi} - Q_{di} = \sum_{l=1}^{n_l} \boldsymbol{M_{PQ}}(i,l) Q_{rl} + \sum_{l=1}^{n_l} \boldsymbol{M_{loss}}(i,l) Q_{lossl} - B_i W_i \tag{4.3}$$

$$W_{sel} - W_{rl} = 2R_l P_{rl} + 2X_l Q_{rl} + R_l P_{lossl} + X_l Q_{lossl} \tag{4.4}$$

$$X_l P_{lossl} - R_l Q_{lossl} = 0 \tag{4.5}$$

$$2\beta_{lossl} W_{rl} \geq P_{rl}^2 + Q_{rl}^2 \tag{4.6}$$

$$\mathbf{C}(lop,l) X_l P_{rl} - \mathbf{C}(lop,l) R_l Q_{rl} = 0 \tag{4.7}$$

Simulation results show that the relaxed inequalities associated with transmission losses are always binding at the optimality provided that there is a feasible solution

to the problem, and cost curves are positive and convex, [37], as well as all LMPs are positive, [62]. Thus, as long as the cost function of generation units is linear (which is convex) and all LMPs at system buses are positive, inequality (4.6) is still binding at the optimality. In above model, $QCF_g(P_g)$ is the cost function of generation units. A practical model for cost function is given in (4.8).

$$QCF_g(P_g) = \nu_g P_g^2 + \tau_g P_g + \delta_g \tag{4.8}$$

where ν_g, τ_g and δ_g are cost coefficients. The quadratic function (4.8) as objective in (4.1) is not consistent with the standard conic optimization format where the objective is required to be linear.

To model the quadratic cost function of generation units, reference [63] proposes a linear approximation of this function. Alternatively, reference [64] adopts a Quadratically-Constrained Quadratic Program (QCQP) to model the quadratic cost function.

Following the past literature, this thesis proposes a conic format of the quadratic cost function. By defining two new variables NT_g and LT_g, the quadratic cost function in (4.8) can be rewritten as:

$$QCF_g(P_g) = NT_g + LT_g \tag{4.9}$$

where NT_g and LT_g are defined as follow:

$$NT_g = \nu_g P_g^2 \tag{4.10}$$

$$LT_g = \tau_g P_g + \delta_g \tag{4.11}$$

It can be straightforwardly proved that we can replace the optimization problem *OPF1*, whose objective is to minimize sum of $\nu_g P_g^2 + \tau_g P_g + \delta_g$ subjected to a set of linear constraints in *OPF1*, with following OPF problem:

OPF2:

$$Minimise \sum_{g \in N_g} NT_g + LT_g \tag{4.12}$$

subject to

$$(\forall i \in N_b,\ \forall l \in N_l)$$

$$P_{gi} - P_{di} = \sum_{l=1}^{n_l} \boldsymbol{M_{PQ}}(i,l) P_{rl} + \sum_{l=1}^{n_l} \boldsymbol{M_{loss}}(i,l) P_{lossl} \tag{4.13}$$

$$Q_{gi} - Q_{di} = \sum_{l=1}^{n_l} \boldsymbol{M_{PQ}}(i,l) Q_{rl} + \sum_{l=1}^{n_l} \boldsymbol{M_{loss}}(i,l) Q_{lossl} - B_i W_i \tag{4.14}$$

$$W_{sel} - W_{rl} = 2R_l P_{rl} + 2X_l Q_{rl} + R_l P_{lossl} + X_l Q_{lossl} \tag{4.15}$$

$$X_l P_{lossl} - R_l Q_{lossl} = 0 \tag{4.16}$$

$$2\beta_{lossl} W_{rl} \geq P_{rl}^2 + Q_{rl}^2 \tag{4.17}$$

$$\mathbf{C}(lop,l) X_l P_{rl} - \mathbf{C}(lop,l) R_l Q_{rl} = 0 \tag{4.18}$$

$$2NT_g \vartheta_g \geq P_g^2 \tag{4.19}$$

where $\vartheta_g = 1/(2\nu_g)$. Now, inequality (4.19) is in the form of a standard convex cone which is consistent with conic optimization format. Doing this, we can solve the AC OPF problem through the convex optimization problem *OPF2*. This can be illustrated by following example. Assume the following problem:

$$\begin{aligned} &Minimise \;\; x^2 \\ &subject\ to \\ &x - y = z + L \\ &\underline{x} \leq x \leq \overline{x} \end{aligned} \tag{4.20}$$

The problem (4.20) can be simply recast as (4.21):

$$\begin{aligned} &Minimise \;\; \xi \\ &subject\ to \\ &x - y = z + L \\ &\underline{x} \leq x \leq \overline{x} \\ &\xi \geq x^2 \end{aligned} \tag{4.21}$$

4.4 The CAC-OPF Problem with Negative LMPs

The physical interpretation of negative LMPs is that increasing loads at some buses can reduce the total generation cost by relieving congestion elsewhere in the network. This allows cheaper generators to output more power and therefore total generation cost to be reduced. There are also some cases where the generation units offer negative bids in their auctions. The German power exchange EEX is one of

these cases, [60, 61]. In this chapter, we only address those cases where physical constraints of the network such as congestion on lines can cause negative LMPs.

As reported in [3], conic relaxation used in modeling transmission losses might not be exact in those cases where there are some system buses with negative LMPs. This can happen through emerging a gap between two sides of relaxed inequality in (4.17). It has been also reported in the literature that other approaches for modeling transmission losses in OPF models such as piecewise linear loss approximation used in DC-OPF models might result in miscalculation of negative LMPs due to occurring breakdown in the solution caused by incorrectly emerging fictitious losses, [62, 65, 66]. The fictitious losses might be emerged if an increase in a load improves the objective function of the problem. This might happen when there are some nodes in the network with negative LMPs. The fictitious losses can fail producing negative LMPs by making these LMPs positive. The impact of the breakdown on LMPs has been investigated and theoretically proven with duality theory and KKT conditions in [65].

In this section, we modify the proposed CAC-OPF to be capable of correctly calculating negative LMPs, if any. We show that proposed conic OPF model i.e. *OPF2* can correctly output negative LMPs by adding a linear term to its objective function. The modified model is given as follows:

OPF3:

$$Minimise \sum_{g\in N_g} NT_g + LT_g + \gamma \sum_{l\in N_l} \beta_{lossl} \tag{4.22}$$

subject to

$$(\forall i \in N_b,\ \forall l \in N_l)$$

$$P_{gi} - P_{di} = \sum_{l=1}^{n_l} \boldsymbol{M_{PQ}}(i,l) P_{rl} + \sum_{l=1}^{n_l} \boldsymbol{M_{loss}}(i,l) P_{lossl} \tag{4.23}$$

$$Q_{gi} - Q_{di} = \sum_{l=1}^{n_l} \boldsymbol{M_{PQ}}(i,l) Q_{rl} + \sum_{l=1}^{n_l} \boldsymbol{M_{loss}}(i,l) Q_{lossl} - B_i W_i \tag{4.24}$$

$$W_{sel} - W_{rl} = 2R_l P_{rl} + 2X_l Q_{rl} + R_l P_{lossl} + X_l Q_{lossl} \tag{4.25}$$

$$X_l P_{lossl} - R_l Q_{lossl} = 0 \tag{4.26}$$

$$2\beta_{lossl} W_{rl} \geq P_{rl}^2 + Q_{rl}^2 \tag{4.27}$$

$$\mathbf{C}(lop,l)X_l P_{rl} - \mathbf{C}(lop,l)R_l Q_{rl} = 0 \tag{4.28}$$

$$2NT_g\vartheta_g \geq P_g^2 \tag{4.29}$$

In the *OPF3*, the objective function has two parts. The first part is the total generation cost and the second term is associated with transmission losses with a penalty factor γ. Note that if $\gamma = 0$, then *OPF3* is equivalent to the *OPF2*. The second term in the objective function ($\gamma \sum_{l\in N_l} \beta_{lossl}$), which is sum of new-defined variables β_{lossl} in the left side of relaxed conic constraint (4.17) forces this inequality to become binding at the optimality in a similar way that we showed in CPF and ECPF models in pervious chapters. In case of using *OPF2*, it might happen that left side of (4.17) gets some values larger than the right side where there are some system buses with negative LMPs. This is because the larger values of left side of (4.17) can result in a lower generation cost. This may create a small gap between the real loss in the network and calculated loss at the optimality especially when there is a congested line where the line flows or bus voltages hit their limits. By modifying the *OPF2* through adding $\gamma \sum_{l\in N_l} \beta_{lossl}$ as the second term in the objective and obtaining *OPF3*, negative LMPs which are associated with active power nodal mismatch constraints can appear in the results. We show this in the simulation results for different cases even for cases where there are congested lines. It should be highlighted that the proposed CAC-OPF in the *OPF2* can correctly output the optimal solution with correct LMPs provided that there is a feasible solution to the problem and all LMPs at system buses are positive, [62]. Otherwise, the *OPF3* can be used where there are some negative LMPs.

4.5 The Case Study and Simulation Results

The CAC-OPF with positive LMPs

Firstly, to evaluate both accuracy and exactness of the conic relaxation in *OPF2* we use different test system. It should be highlighted that in this section LMPs at all system buses are positive.

First a simple 4 bus test system used in chapter 3 is used (See Figure 3.1). Three different line flow limits are tested. In the first run, there is not any upper limit on the line flows and therefore none of the lines become congested. In the second run, we introduce a $60MVA$ line limit on line 1 to make this line congested. Finally, for the third run, upper limit for line 3 is set at $30MVA$ to become congested. The results of proposed OPF formulation are then fed into MATPOWER [67] to compare the optimal loss obtained in the conic model with loss calculated from a standard Full AC OPF (FAC-OPF) model in MATPOWER ($P_{loss,FAC}$). Results obtained from Conic OPF in GAMS using MOSEK solver [39] and MATPOWER are given in Table 4.1.

Secondly, to apply the model on larger test systems, 14, 30, 57 and 118 IEEE test systems are used. A summary of the obtained results are given in Table 4.2. In all these simulations some of the lines are forced to hit their limits. In these Tables, $P_{loss,real}$ is the sum of the transmission line losses i.e. right sides of $P_{lossl} \geq \frac{P_{rl}^2+Q_{rl}^2}{V_{rl}^2}R_l$ and P_{lossl} is the sum of left sides of this relaxed inequality at the optimal solution. Results in Tables 4.1 and 4.2 show that the conic relaxation is exact

Table 4.1: The CAC-OPF and FAC-OPF results for a 4-bus test system when lines L1 and L3 are congested

Lines' Limits (MVA)	No Limit	L1=60	L3=30
$P_{lossl}(MW)$	3.605	3.829	5.849
$P_{loss,real}(MW)$	3.605	3.829	5.849
$P_{loss,FAC}(MW)$	3.583	3.812	5.810

Table 4.2: Comparison between CAC-OPF and FAC-OPF models to show the accuracy and exactness of conic relaxation

IEEE Test System	14	30	57	118
$P_{lossl} - P_{loss,real}$ (%)	0	0	0	0
$P_{lossl} - P_{loss,FAC}$ (%)	0.43	0.228	0.479	0.001

even in case of an extremely congested network.

As it is observed from the results both sides of the relaxed inequalities are always identical meaning that the inequality is always binding at the optimality. Very small difference between outputs of full AC and conic models ($P_{loss,FAC}$ and P_{lossl}) stems from approximations we used to render the phase angle constraints linear.

The CAC-OPF with negative LMPs

In this section, the CAC-OPF model in *OPF3* is tested on a modified version of IEEE 30 bus test system (See Figure 4.2). Two cases with no congested line (NCL) and with a congested line (CL) in the network are studied. The capacity of generation units and associated cost coefficients are modified and set out as given in Table 4.3 in order to obtain negative LMPs. In this section, we assume that cost coefficients except τ_g are equal to zero.

In the first case, no limits on power flows are set. In the second case, we force the line between buses 4 and 6 to hit an upper limit of $30MW$ and then investigate

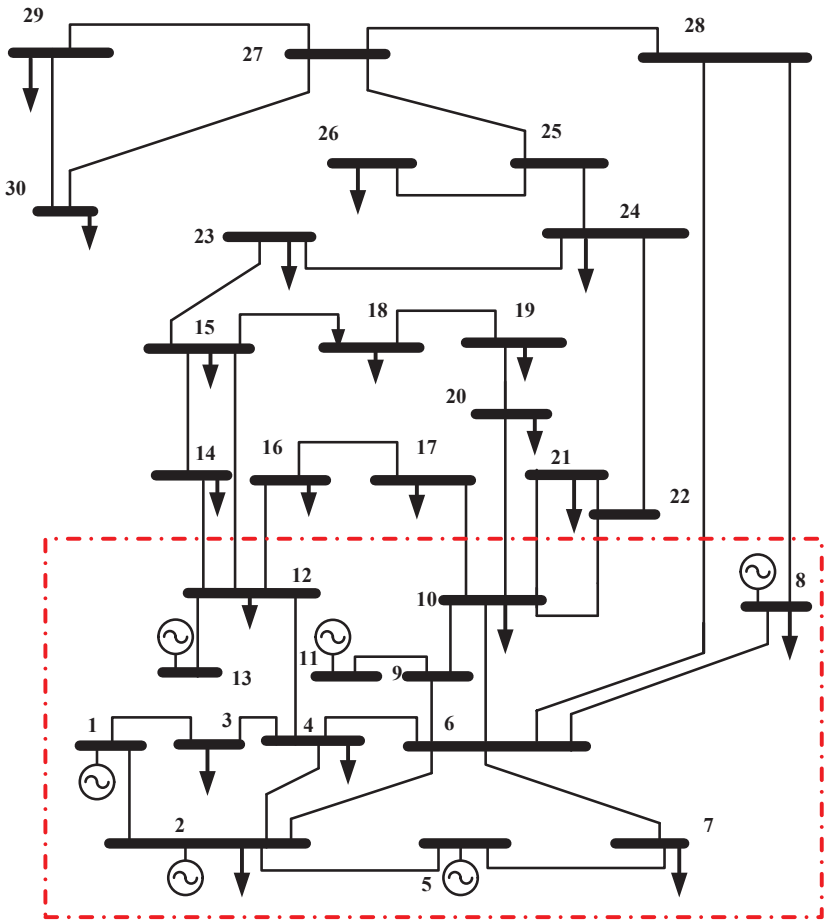

Figure 4.2: The IEEE 30 bus test system.

the impact of congestion on emerging negative LMPs. For the case where there is no congested line, obtained results from both CAC-OPF and the FAC-OPF for the first 11 buses, within the dashed area illustrated in Figure 4.2, are given in Figure 4.3. The LMPs for the same buses in the second case (i.e. with congested line) obtained from both models are given in Figure 4.4.

As it is observed from the results, LMPs of buses 3 and 4 are positive $38\$/MWh$ and $39\$/MWh$, respectively, in the first case where there is no congested line in the system. However, in the second case where the line (4,6) gets congested, LMPs of buses 3 and 4 become $-2.2\$/MWh$ and $-6.2\$/MWh$, respectively. This means

Table 4.3: Modified IEEE 30 bus test system generator parameters

	P_g^M (MW)	τ_g $(\$/MW)$
G1	160	15
G2	60	20
G5	40	40
G8	40	40
G11	30	40
G13	30	40

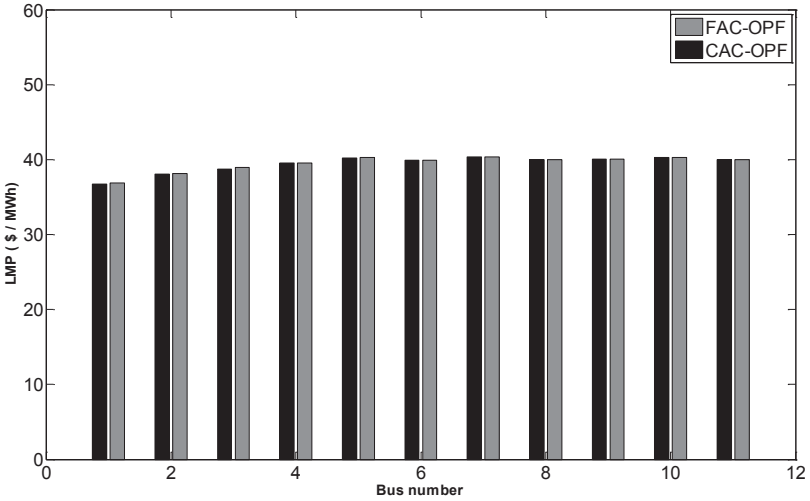

Figure 4.3: The LMPs of system buses in the dashed area shown in Figure 4.2 with no congested line .

increasing loads at these buses can result in a lower total generation cost. These results illustrate a good accuracy of the proposed formulation in calculating LMPs at system buses for both cases with and without negative LMPs.

To show the impact of these negative LMPs on the generation cost, we increase the loads at buses 3 and 4 which have negative LMPs to $7MW$ and $15MW$, respectively. Dispatch results are given in Table 4.5. As it is seen from the results, increased loads at buses with negative LMPs result in more production from cheaper generator 1. This in turn results in a lower total generation cost. It should be high-

Table 4.4: The Modified CAC-OPF results for IEEE 30 test system from proposed formulation, NCL indicates a case with no congested line and CL indicates a case with a congested line (4,6)

AC Bus	P_{gi}(MW)	LMP($/MWh)	
1	160.000	36.755	NCL
	130.963	15.000	CL
2	60.000	38.097	NCL
	60.000	21.774	CL
3	-	38.708	NCL
	-	**-2.268**	CL
4	-	39.546	NCL
	-	**-6.203**	CL
5	40.000	40.240	NCL
	29.546	40.000	CL
6	-	39.932	NCL
	-	55.813	CL
7	-	40.336	NCL
	-	49.706	CL
8	25.580	40.000	NCL
	40.000	55.592	CL
9	-	40.049	NCL
	-	45.469	CL
10	-	40.254	NCL
	-	40.013	CL
11	6.487	40.000	NCL
	30.000	45.334	CL
Total	**Cost**	6482.719	NCL
	($)	7146.308	CL

lighted that in all these cases the relaxed conic constraints are always binding and active at the optimality.

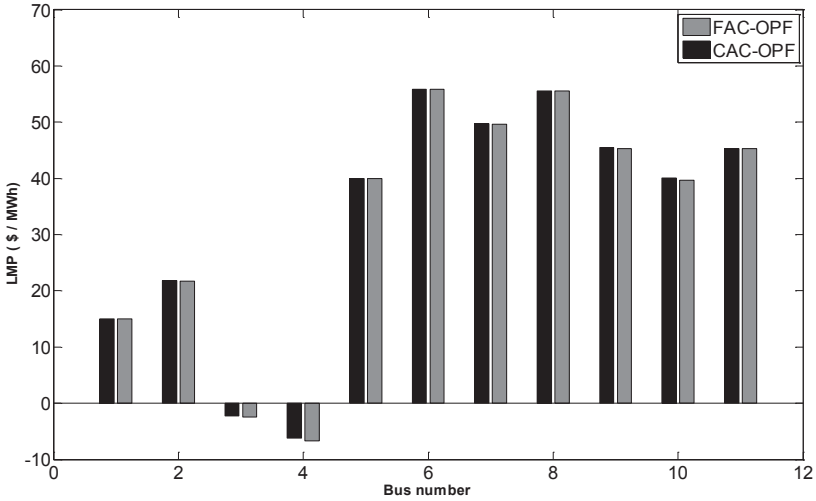

Figure 4.4: The LMPs of system buses in the dashed area shown in Figure 4.2 with a congested line.

Table 4.5: The OPF results for IEEE 30 Test System, CL indicates a case with a congested line (4,6), CL-IL indicates a case with a congested line and increased loads at buses 3 and 4

	P_{g1} (MW)	P_{g2} (MW)	P_{g5} (MW)	P_{g8} (MW)	P_{g11} (MW)	P_{g13} (MW)	Cost ($)
CL	130.96	60.00	29.54	40.00	30.00	0.00	7146.30
CL-IL	155.03	60.00	19.15	40.00	30.00	0.00	7091.84

Part III

Hybrid AC-DC Network Analysis

Chapter 5

Conic Optimization Problem for AC Grids with Embedded VSC-DC Grids and Shunt FACTS Devices

5.1 Introduction

Before identifying benefits of VSC-DC grids and FACTS devices, they need to be properly modeled in analytical tools such as optimization models. In this chapter, firstly, equations associated with these devices are derived and then transformed into the conic format. Then, a Conic AC-DC OPF (CAD-OPF) model is proposed.

5.2 Background

Recently, several changes in power systems have brought many challenges to the traditional AC power systems. These changes result mostly from the power system expansion, fast increasing of power consumption, emerging renewable energy sources, and power systems interconnections. These can lead to more frequent congestion and overloading in power system components. On the other hand, if the high-carbon generating units are used to respond to the increasing power demand, the carbon dioxide in the atmosphere will increase which has a negative effect on both climate and society.

The smart-grid technologies were proposed to overcome these new challenges in an efficient, reliable, and economic way. These technologies allow integrating

the low-carbon generating units, flexible AC components, and renewable energy sources into the power systems in such a way that power systems operate in their full capacity in an economically efficient way, [68].

Two technologies, HVDCs and the Flexible AC Transmission Systems (FACTS), are perfectly suited to respond to the mentioned challenges. For instance, the FACTS technology can make the full capacity of the existing system available for transferring more electrical power to demand locations (a substitute for high-carbon local generating units). Perfect characteristics of the new generation of HVDC technology, Voltage Source Converter based HVDC (VSC-HVDC), have made it an essential technology for integrating more low-carbon generating units.

Both HVDC and FACTS devices can bring several benefits to power systems such as helping to improve congestion problems in a heavily loaded system, [69], increasing the transfer capacity and stability of the system, minimizing the transmission losses, energy savings, and reducing the carbon dioxide. Therefore, the future smart grids inevitably consist of such flexible hybrid AC-DC systems, [70]. However, smart utilization of these technologies requires a smart tuning of their settings. This in turn needs a proper modeling of these devices in the power system analysis programs. So far, these devices have been mostly modeled in the Load Flow and Optimal Power Flow problems through deriving a set of nonlinear equations, [71–77].

One of the benefits achieved from these flexible components is the energy loss minimization which can result in improving the transmission system efficiency, [78]. The transmission losses superimpose to the total demand and extra generation is required. These losses form 3.5% of total power generation, [79]. In an assessment performed in US, the annual monetary value associated with T&D losses is $21 billion (based on the average national retail price of electricity and the total T&D losses in 2005 [79]).

In another study, the potential improvement in the energy efficiency through the loss reduction is estimated to be higher than 1% of total delivered energy which means an annual saving of $3, [78]. In this regard, several works have proposed different techniques to directly minimize the losses. In reference [80], a primal-dual interior-point method has been used to formulate an optimization problem with loss minimization objective. Authors in reference [81] have proposed a predictor-corrector modified barrier approach based on Newton's method. Another group of researchers have tried to develop the loss minimization problem through the non-deterministic search techniques due to their excellent global search characteristics, [82, 83].

Several works have investigated the impact of FACTS and back-to-back HVDC on transmission losses. Reference [84] has investigated the impact of back-to-back VSC-type HVDC systems on the meshed network losses. In this reference a Newton-Raphson (NR) Load Flow program is employed to assess the network losses. This means the HVDC parameters have to be set before running the program and then loss is calculated with the pre-set parameters. Authors in reference [85] have studied the impact of VAr optimization using coordinated SVC on loss minimization.

A conventional nonlinear OPF has been used in this study. Reference [86] has analyzed the impact of UPFC on optimal reactive power dispatch by successively solving the steady-state power flows and optimal tuning of reactive power control variables. In reference [87], parameters of some FACTS devices have been added to the control variables to study their impacts on system loss minimization. However, this reference is mainly focused on series FACTS devices. To the author's knowledge, reference [88] is the only work which has recently studied the impact of embedded multi-terminal VSC-HVDC systems on transmission losses however without any account of FACTS devices. In this reference, the conventional nodal mismatch power flow equations are used to form the OPF problem. It is assumed in this reference that there is no relation between DC and AC bus voltages at the converter station where they are usually linked by modulation index. Since those devices with reactive power injection/absorption capability have the most contribution to the loss minimization, the present chapter addresses AC grids with embedded VSC-type DC grids, STATCOM, and SVC devices.

In this chapter, a Conic AC-DC OPF (CAD-OPF) problem is proposed to minimize the ohmic losses (both in AC and DC grids) by optimally tuning of settings of installed VSC-DC grids, STATCOM, and SVCs. For power flow equations associated with AC grid we use derived equations from pervious chapters. Then, technical constraints associated with DC grid, VSC stations (in both VSC-DC grid and STATCOM), and SVCs are derived as functions of variables used in the conic format. This way, constraints associated with VSC and SVC are embedded in the conic problem.

In this thesis, unlike reference [88], the relation between AC and DC sides are considered through both bus voltage and active power variables. Different control modes for installed VSC-DC stations, STATCOMs and SVCs are taken into account to study their impacts on the transmission losses.

5.3 Mathematical Model

AC Network

Considering active/reactive power injection of VSC-HVDCs, VSC-STATCOMs, and SVCs (See Figures 5.1 and 5.3), AC power flow equations are as follows:

$$(\forall i \in N_b,\ \forall l \in N_l)$$

$$P_{gi} - P_{di} + P_{Ci} + P_{L,swi} = \sum_{l=1}^{n_l} \boldsymbol{M_{PQ}}(i,l) P_{rl} + \sum_{l=1}^{n_l} \boldsymbol{M_{loss}}(i,l) P_{lossl} \qquad (5.1)$$

$$Q_{gi} - Q_{di} + Q_{Ci} + Q_{STATi} + Q_{SVCi} = \sum_{l=1}^{n_l} \boldsymbol{M_{PQ}}(i,l) Q_{rl} + \sum_{l=1}^{n_l} \boldsymbol{M_{loss}}(i,l) Q_{lossl} - B_i W_i \tag{5.2}$$

$$W_{sel} - W_{rl} = 2R_l P_{rl} + 2X_l Q_{rl} + R_l P_{lossl} + X_l Q_{lossl} \tag{5.3}$$

$$X_l P_{lossl} - R_l Q_{lossl} = 0 \tag{5.4}$$

$$2\beta_{lossl} W_{rl} \geq P_{rl}^2 + Q_{rl}^2 \tag{5.5}$$

$$\mathbf{C}(lop,l) X_l P_{rl} - \mathbf{C}(lop,l) R_l Q_{rl} = 0 \tag{5.6}$$

where P_{Ci} and Q_{Ci} are injected/absorbed active and reactive powers of VSCs at PC buses shown in Figure 5.1. Q_{STATi} and Q_{SVCi} are injected/absorbed reactive powers of STATCOMs and SVCs at their connection points shown in Figure 5.3, respectively. $P_{L,swi}$ is the active power loss of STATCOM absorbed from the AC grid.

DC Network and VSC Stations

To derive the line flow equations for the DC grid and associated VSC stations, the equivalent circuit of a DC line and its associated VSC station shown in Figure 5.1 is considered.

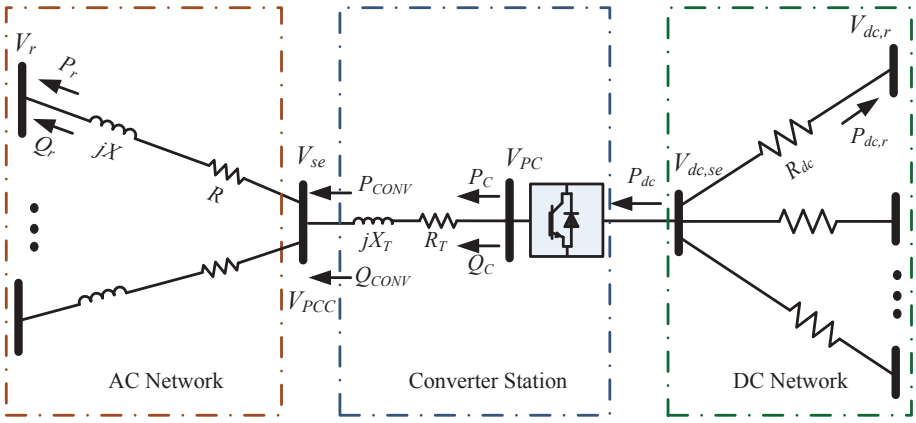

Figure 5.1: AC lines, VSC station, and DC lines equivalent models .

Derived equations are listed in order.
Mismatch equations at each DC node:

$$(\forall i \in N_b^{dc},\ \forall s \in S,\ \forall l \in N_l^{dc}, W_{dc} = V_{dc}^2)$$
$$P_{dc,i} = -\sum_{l=1}^{n_l^{dc}} \boldsymbol{M_{P_{dc}}}(i,l) P_{dc,rl} - \sum_{l=1}^{n_l^{dc}} \boldsymbol{M_{loss,dc}}(i,l) P_{dlossl} \tag{5.7}$$

where n_l^{dc} is the number of DC buses and N_b^{dc} is the set of DC buses. $P_{dc,i}$ is the injected/absorbed power at each DC bus ($i \in N_b^{dc}$). The $\boldsymbol{M_{P_{dc}}}$ and $\boldsymbol{M_{loss,dc}}$ are incidence matrices associated with DC grid which are obtained in a similar way that $\boldsymbol{M_{PQ}}$ and $\boldsymbol{M_{loss}}$ were obtained for the AC grid. $P_{dc,rl}$ is the DC line flow at receiving end of each DC line ($l \in N_l^{dc}$).
Power loss at each DC link:

$$P_{dlossl} = \frac{P_{dc,rl}^2}{V_{dc,rl}^2} R_{dc,l} \tag{5.8}$$

DC voltage drop across each DC link:

$$W_{dc,sel} - W_{dc,rl} = (2P_{dc,rl} + P_{dlossl}) R_{dc,l} \tag{5.9}$$

where $W_{dc,sel}$ and $W_{dc,rl}$ are square of bus voltages at sending and receiving ends of each DC line, respectively. As proposed in pervious chapters, here equality (5.8) is also replaced with an inequality and rewritten as follows:

$$2\beta_{dlossl} W_{dc,rl} \geq (P_{dc,rl})^2 \tag{5.10}$$

where $P_{dlossl} = 2R_{dcl}\beta_{dlossl}$. Constraint (5.10) is now in the form of rotated convex cone.
AC and DC sides coupling:
The relation between AC and DC sides are represented by both voltage and power couplings. As it is shown in Figure 5.2, DC side voltage at each station is related to AC side voltage by (5.11).

$$V_{pc,i} = \frac{V_{dc,i}}{2\sqrt{2}} m_C \tag{5.11}$$

where m_C is the modulation index in each converter, which in practice it is limited to $m_{C,m} \leq m_C \leq m_{C,M}$ where $m_{C,m} = 0.5$ and $m_{C,M} = 1$. Squaring (5.11) and using $m^2_{C,m} \leq m^2_C \leq m^2_{C,M}$, one can obtain following linear expressions ($W_{pc} = V^2_{pc}$):

$$8W_{pc,i} - m^2_{C,M} W_{dc,i} \leq 0 \tag{5.12}$$

$$m^2_{C,m} W_{dc,i} - 8W_{pc,i} \leq 0 \tag{5.13}$$

Converter losses:
Several steady state loss models for VSC converters have been used in the literature, [76, 89]. In this thesis we consider the loss model proposed in [89] where the converter losses are represented by a series resistor (R_{Cse}) on the AC side and a shunt one (R_{Csh}) on the DC side (See Figure 5.2). It should be noted that in case converter losses are represented by a series reactance as well, it can be easily lumped to the transformer reactance. Here, the series resistance R_{Cse} is also lumped into the series transformer resistance. The associated loss with shunt resistance can be written as:

$$P_{lshi} R_{Csh} = W_{dc,i} \tag{5.14}$$

Having calculated the shunt term of converter losses by (5.14), active power at converter bus (n_{PC}) can be obtained by (5.15).

$$P_{Ci} = P_{dc,i} - P_{lshi} \tag{5.15}$$

Associated equations for the AC side of each station are derived using the equivalent circuit shown in Figure 5.2. As it is seen, coupling transformer and phase reactance can be simply modelled as an AC line.

STATCOM

In a similar way the coupling transformer between the VSC-STATCOM and its connection point to the network can be modeled as an AC line (See Figure 5.3). A shunt resistance $R_{ST,sh}$ at the DC side of the VSC-STATCOM is also used to model switching losses. The DC side voltage of STATCOM is coupled to the AC side voltage by (5.16).

$$V_{STAT} = \frac{V_{dc,ST}}{2\sqrt{2}} m_{ST} \tag{5.16}$$

where m_{ST} is the modulation index of STATCOM. Squaring (5.16) and using $m^2_{ST,m} \leq m^2_{ST} \leq m^2_{ST,M}$, one can obtain following linear expressions ($W_{STAT} = V^2_{dc,ST}$):

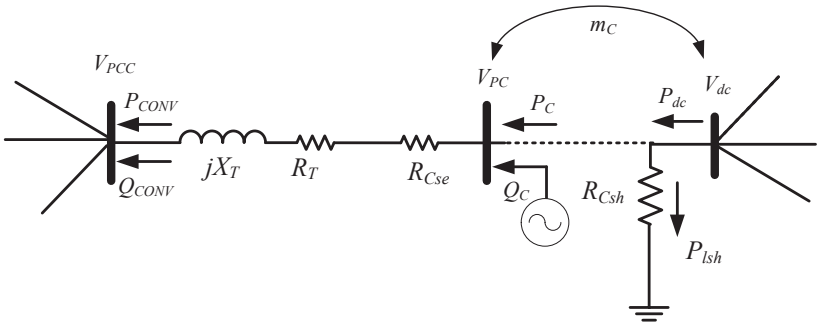

Figure 5.2: The VSC stations equivalent circuit.

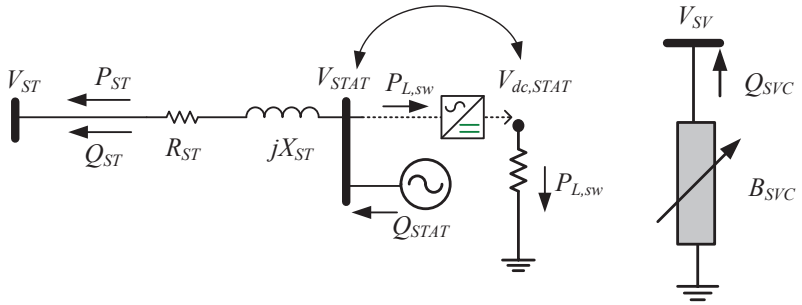

Figure 5.3: The STATCOM and SVC equivalent circuits.

$$8W_{STAT} - m_{ST,M}^2 W_{dc,ST} \leq 0 \tag{5.17}$$

$$m_{ST,m}^2 W_{dc,ST} - 8W_{STAT} \leq 0 \tag{5.18}$$

where $m_{ST,m}$ and $m_{ST,M}$ are minimum and maximum bounds of the modulation index. The switching losses are calculated as follows:

$$P_{L,sw} = \frac{W_{dc,ST}}{R_{ST,sh}} \tag{5.19}$$

SVC

The SVC model is shown in Figure 5.3. In this model, the SVC is modeled as a variable susceptance with upper and lower bounds, [74]. Accordingly, SVC is modeled by following constraints ($W_{SVi} = V_{SVi}^2$).

$$Q_{SVC} = B_{SVC} W_{SV} \tag{5.20}$$

$$B_{SVC,m} \leq B_{SVC} \leq B_{SVC,M} \tag{5.21}$$

where $B_{SVC,m}$ and $B_{SVC,M}$ are minimum and maximum bounds of SVC susceptance. From (5.20) and (5.21), we can obtain:

$$B_{SVC,m} \leq \frac{Q_{SVC}}{W_{SV}} \leq B_{SVC,M} \tag{5.22}$$

Inequality (5.22) can be written through two following inequalities:

$$\begin{aligned} Q_{SVC} - B_{SVC,M} W_{SV} &\leq 0 \\ -Q_{SVC} + B_{SVC,m} W_{SV} &\leq 0 \end{aligned} \tag{5.23}$$

5.4 Optimization Problem

Now we can formulate a Conic AC-DC OPF (CAD-OPF) in which both AC and DC losses are minimized and all AC and DC technical constraints are taken into account:

$$Minimize \sum_{l \in N_l} P_{lossl} + \sum_{l \in N_l^{dc}} P_{dlossl} \tag{5.24}$$

$$subject\ to \tag{5.25}$$

$(\forall i \in N_b,\ \forall l \in N_l)$

$$P_{gi} - P_{di} + P_{Ci} + P_{L,swi} = \sum_{l=1}^{n_l} \boldsymbol{M_{PQ}}(i,l) P_{rl} + \sum_{l=1}^{n_l} \boldsymbol{M_{loss}}(i,l) P_{lossl} \tag{5.26}$$

$$Q_{gi} - Q_{di} + Q_{Ci} + Q_{SVCi} + Q_{STATi} = \sum_{l=1}^{n_l} \boldsymbol{M_{PQ}}(i,l) Q_{rl} + \sum_{l=1}^{n_l} \boldsymbol{M_{loss}}(i,l) Q_{lossl} - B_i W_i \tag{5.27}$$

$$W_{sel} - W_{rl} = 2R_l P_{rl} + 2X_l Q_{rl} + R_l P_{lossl} + X_l Q_{lossl} \tag{5.28}$$

$$X_l P_{lossl} - R_l Q_{lossl} = 0 \tag{5.29}$$

$$2\beta_{lossl} W_{rl} \geq P_{rl}^2 + Q_{rl}^2 \tag{5.30}$$

$$\mathbf{C}(lop,l) X_l P_{rl} - \mathbf{C}(lop,l) R_l Q_{rl} = 0 \tag{5.31}$$

$$(P_{rl})^2 + (Q_{rl})^2 \leq CAP_{Rl}^2 \tag{5.32}$$

$$W_i^m \leq W_i \leq W_i^M \tag{5.33}$$

$$P_{gi}^m \leq P_{gi} \leq P_{gi}^M \tag{5.34}$$

$$Q_{gi}^m \leq Q_{gi}, \leq Q_{gi}^M \tag{5.35}$$

$(\forall i \in N_b^{dc},\ \forall l \in N_l^{dc})$

$$P_{dc,i} = -\sum_{l=1}^{n_l^{dc}} \boldsymbol{M_{P_{dc}}}(i,l) P_{dc,rl} - \sum_{l=1}^{n_l^{dc}} \boldsymbol{M_{loss,dc}}(i,l) P_{dlossl} \tag{5.36}$$

$$W_{dc,sel} - W_{dc,rl} = (2P_{dc,rl} + P_{dlossl}) R_{dc,l} \tag{5.37}$$

$$2\beta_{dlossl} W_{dc,rl} \geq (P_{dc,rl})^2 \tag{5.38}$$

$$8W_{pc,i} - m_{C,M}^2 W_{dc,i} \leq 0 \tag{5.39}$$

$$m_{C,m}^2 W_{dc,i} - 8W_{pc,i} \leq 0 \tag{5.40}$$

$$P_{lshi} R_{Csh} = W_{dc,i} \tag{5.41}$$

$$P_{Ci} = P_{dc,i} - P_{lshi} \tag{5.42}$$

$$(P_{Ci})^2 + (Q_{Ci})^2 \leq CAP_{Ci}^2 \tag{5.43}$$

$$W_{dc,i}^{m} \leq W_{dc,i} \leq W_{dc,i}^{M} \tag{5.44}$$

$$(\forall i \in N_b^{ST})$$
$$8W_{STAT,i} - m_{ST,M}^2 W_{dc,STi} \leq 0 \tag{5.45}$$

$$m_{ST,m}^2 W_{dc,STi} - 8W_{STAT,i} \leq 0 \tag{5.46}$$

$$P_{L,swi} R_{ST,shi} = W_{dc,STi} \tag{5.47}$$

$$(\forall i \in N_b^{SV})$$
$$Q_{SVCi} - B_{SVC,M} W_{SVi} \leq 0 \tag{5.48}$$

$$-Q_{SVCi} + B_{SVC,m} W_{SVi} \leq 0 \tag{5.49}$$

where N_b^{SV} and N_b^{ST} are sets of SVC and STATCOM connected buses, respectively. The W^m and W^M are limits on the AC bus voltages. The P_g^m and P_g^M are bounds on active power production of generation units. The Q_g^m and Q_g^M are bounds on reactive power production of generation units. The W_{dc}^m and W_{dc}^M are bounds on the DC bus voltages. The CAP_C is the capacity of VSC converters. The inequality (5.32) represents the limits on transmission power flows and CAP_{Rl} is the capacity of each line.

This CAD-OPF is a convex optimization problem. The CAD-OPF is subjected to a set of constraints involving a set of linear equalities and inequalities accompanied by some nonlinear constraints which are in the form of convex cones (the two sets of rotated quadratic cone: (5.30) and (5.38) and two sets of quadratic cone: (5.32) and (5.43), [35, 36]).

5.5 Case Study and Simulation Results

To evaluate the proposed CAD-OPF formulation for minimizing the network losses for a hybrid AC-DC grid, the IEEE 30-bus test system is modified and used. The objective function of this optimization problem as given in (5.24) is the total network losses in both AC and DC grids.

We assume that two three-terminal DC grids, two STATCOMs and two SVCs have been already installed in the grid as shown in Figure 5.4. Parameters of the VSC stations and the DC grids are given in Table 5.1.

We assume that electricity market operator runs a day-ahead market. He runs a security-constrained bid-based economic dispatch. The economic dispatch level of

Table 5.1: VSC Station and DC Grid Parameters

Parameter	R_T R_{ST}	X_T X_{ST}	R_{Csh} $R_{ST,sh}$	R_{Cse} $R_{ST,se}$	R_{DC}
(p.u.)	0.01	0.1	10e4	0.05	0.03

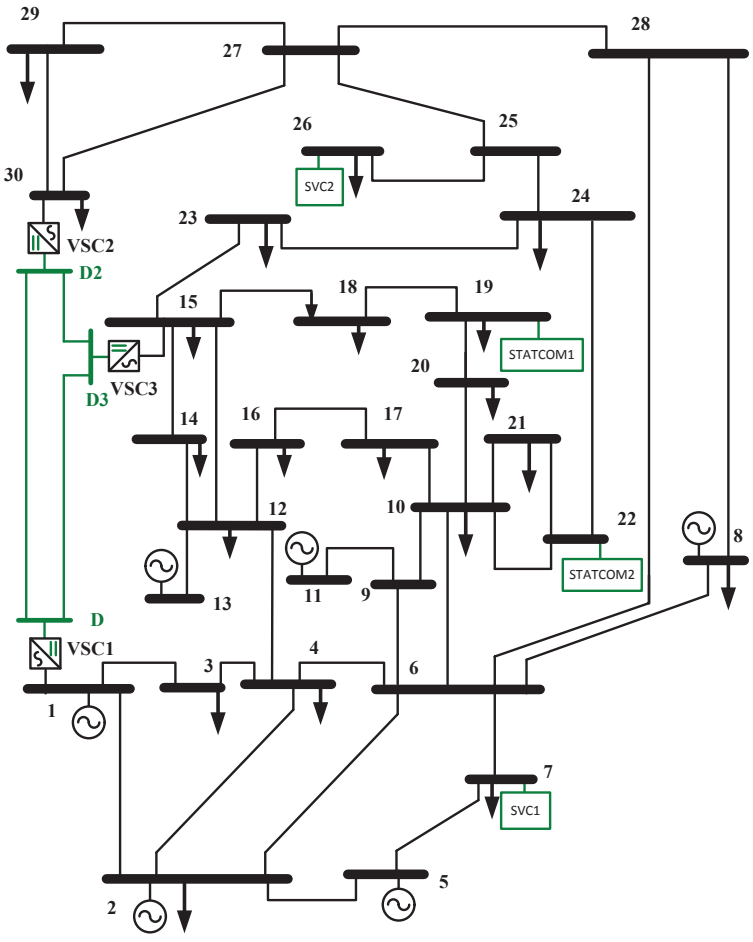

Figure 5.4: The IEEE 30-bus test system embedded with DC grid, STATCOM, and SVC.

each generating unit is determined in day-ahead market. We assume also the transmission system operator is responsible for the real-time operation of power system. He runs a balancing market to handle the shocks in the system and also minimize the ohmic losses in the whole AC-DC transmission system. For the ohmic loss minimization, the transmission system operator uses the economic dispatch level of all generating units calculated in the day-ahead market. To model this process, first we run a DC-OPF using MATPOWER to obtain the economic dispatch of generation units. We use these generation levels obtained from DC-OPF as scheduled generation. Running the DC-OPF for IEEE 30-bus test system gives us the generation levels of $200.62MW$ for generator 1 and $82.78MW$ for generator 2. We set these values as generation levels of generators 1 and 2 in our conic optimization model. Then we run CAC-OPF for the pure AC system to obtain the minimum active power losses. As given in Table 5.2, the minimized ohmic loss through the CAC-OPF is equal to **15.798 MW**. In order to show the accuracy of the CAC-OPF, we again run the load flow program using MATPOWER with preset values obtained in CAC-OPF. This load flow gives us a calculated loss value of **15.793 MW**. As it was perviously explained, this small error comes from the approximations used in our model.

Table 5.2: Ohmic losses in both AC and AC-DC networks

(MW)	$\sum P_{L,swi}$	$\sum P_{lshi}$	$\sum P_{dlossl}$	$\sum P_{lossl}$
Original	-	-	-	15.798
Network	-	-	-	
Case 1	0.18022	0.60678	0.10857	18.008
Case 2	0.16277	0.60738	0.01890	21.676
Case 3	0.16420	0.71984	0.02994	12.085
Case 4	0.16939	0.39632	0.01788	11.348
Case 5	0.17311	0.71983	0.03989	10.004
Case 6	0.14853	0.71940	0.14257	25.427

In the next step we run the CAD-OPF incorporating HVDC links and FACTS devices to study their impacts on the active power losses. Six cases are studied as follow:

- ***Case 1)*** In this case, converters 1 and 2 are set to be in the PQ mode and converter 3 is chosen as slack station to keep the voltage of bus D1 at $4.5p.u.$ Converter 1 is set to control active and reactive powers in $70MW$ and $-10MVar$ and Converter 2 is trying to control active and reactive powers in $50MW$ and $5MVar$. All parameters of STATCOM and SVC devices are free to get any value within their operational areas. In this case there is no limit on power flow through the DC lines. The ratings of converters in this case are chosen as $150MVA$.

Table 5.3: Optimal injected/absorbed powers of VSC-DC grid (active and reactive powers are in (MW) and ($MVar$), respectively. * shows the preset values)

	P_{C1}	P_{C2}	P_{C3}	Q_{C1}	Q_{C2}	Q_{C3}
Case 1	-120.715	70*	50*	-10*	5*	-9.875
Case 2	-20.626	50*	-30*	-24.294	-3.497	25.181
Case 3	-67.485	19.153	47.582	-18.591	0.229	-1.233
Case 4	-39.822	19.240	20.168	-12.549	3.648	6.593
Case 5	-77.666	21.355	55.550	-7.291	3.356	10.699
Case 6	-149.809	92.805	56.142	7.559	7.604	31.563

Table 5.4: Optimal injected/absorbed powers of STATCOM and SVCs.

	Q_{STAT1}	Q_{STAT2}	Q_{SVC1}	Q_{SVC2}
Case 1	15.361	7.840	13.240	23.846
Case 2	13.731	7.842	4.886	11.066
Case 3	15.695	10.417	5.813	39.490
Case 4	6.681	4.332	3.108	11.607
Case 5	6.476	4.680	3.001	11.242
Case 6	-9.057	-7.373	6.168	24.090

Table 5.5: Optimal settings of installed SVCs for all cases

	case 1	case 2	case 3	case 4	case 5	case 6
$B_{SVC1}(p.u.)$	0.118	0.051	0.058	0.030	0.028	0.065
$B_{SVC2}(p.u.)$	0.216	0.118	0.395	0.111	0.107	0.233

- ***Case 2)*** Converters 1 and 2 are set to be in the PV mode and converter 3 is chosen as slack station to keep the voltage of bus D1 at $4.5p.u.$ and its AC voltage at PCC at $1p.u.$ Converter 1 is set to control active and reactive powers in $50MW$ and AC voltage of PCC at $1p.u.$ and Converter 2 is trying to control active and reactive powers in $-30MW$ and AC voltage of PCC at 1 p.u. In this case all parameters of STATCOM and SVC devices are free to get any value within their operational areas. In this case there is no limit on power flow through the DC lines. The ratings of converters in this case are chosen as $150MVA$.

- ***Case 3)*** All Converters, STATCOMs, and SVCs are set to control the AC

bus voltage at $1p.u.$ Other converter parameters are free to get any value in their operational areas. In this case there is no limit on power flow through the DC lines. The ratings of converters in this case are reduced to $70MVA$.

- ***Case 4)*** All control variables of the converters and FACTS devices are free to get any value within their operational areas while the power flow on the DC lines are limited to $20MW$. The rating of converters in this case is chosen as $70MVA$.

- ***Case 5)*** All parameters are free to get any value within their operational areas. The ratings of converters are chosen as $150MVA$ and DC line power flow limits are chosen as $50MW$.

Congestion on the Lines: We study another case (***Case 6***), to show the exactness of the conic relaxation for cases where some lines are congested. We put three hard limits on three lines in these test systems. The limits of $30MVA$, $18MVA$ and $45MVA$ are set for lines (4,6), (10,21) and (27,28), respectively. Again all VSC and FACTS parameters are free to get any value within their limits. The ratings of converters are chosen as $150MVA$

In all simulations, V_i^m and V_i^M are set at **0.94** and **1.06** $p.u.$, respectively. The voltage bus at the converter buses are set at **0.9** and **1.1** $p.u.$, respectively. The modulation index limits are set at 0.5 and 1. Therefore, base on (5.11) and V_{pc} limits, the DC voltage limits should be **2.54** and **6.22** $p.u.$ However these limits are arbitrarily chosen as **2.7** and **4.9** $p.u.$

Table 5.6: DC side voltages of VSC-DC grid and STATCOMs (* shows the preset values)

$(p.u.)$	$V_{dc,1}$	$V_{dc,1}$	$V_{dc,1}$	$V_{dc,STAT1}$	$V_{dc,STAT2}$
Case 1	4.50000*	4.49576	4.49621	3.00920	2.99450
Case 2	4.50000*	4.49843	4.50021	2.86149	2.84411
Case 3	4.89981	4.89804	4.89746	2.87254	2.85799
Case 4	3.63572	3.63409	3.63407	2.91664	2.90380
Case 5	4.90000	4.89798	4.89728	2.93813	2.94586
Case 6	4.89998	4.89502	4.89577	2.70636	2.74376

The results associated with ohmic losses in the whole AC-DC network are given in Table 5.2. As it is observed the proposed CAD-OPF outputs comprehensive knowledge about all lossy elements of the grid. Tables 5.3 and 5.4 show all optimal injected/absorbed active and reactive powers of devices for all cases. As it is observed the lowest AC transmission loss is achieved from ***Case 5*** where all parameters of VSC stations, STATCOMs and SVCs are free to get any value within

their operational limits. This corresponds to **36.7%** reduction in losses as compared to original AC system. Contrarily, through an improper pre-setting of these devices considered in ***Case 1*** and ***2*** transmission losses are considerably increased as compared to the losses in the pure AC network (**13.9%** increase in losses as compared to original AC system).

Table 5.5 shows the optimal setting for the installed SVC devices. Table 5.6 also shows the optimal DC side voltages of both installed DC girds and STATCOMs at the optimality.

It should be reported that in ***Cases 1*** to ***5***, where there is no congested line, conic relaxations used in the CAD-OPF are always exact at the optimality (binding inequalities). In ***Case 6***, all three selected lines hit their limits and get congested. As it was expected even with these congested lines conic relaxations used in the CAD-OPF are exact at the optimality.

This chapter presents a convex AC-DC OPF (based on Conic Programming) with embedded VSC-DC grids, STATCOM, and SVCs, which have the highest impact on the transmission losses. Both accuracy and exactness of proposed relaxations used in the CAD-OPF are evaluated on different test systems. Through the proposed formulation, optimal settings of VSC-DC grids and shunt FACTS devices are determined. Results show that in addition to generators, these devices can contribute to minimize ohmic losses by optimal tuning of their control variables. The simulation results also show that an improper pre-setting of these devices can result in considerably high active power losses.

Chapter 6

Optimization of Wind Power Penetration in Hybrid AC-DC Networks

6.1 Introduction

This chapter addresses one of the challenges which power systems experience as a result of intermittent nature of wind power output. This is done by modifying perviously proposed CAD-OPF model to be adopted by power system operators to ensure a certain voltage stability margin for the wind power realization in the real-time operation. The objective of the proposed optimization model is to maximize the wind power injection to the grid by optimal tuning of VSC-HVDC links connecting wind farm DC grids to the main AC grid.

6.2 Background

Integration of renewable energy sources into power systems is increasing throughout the world due to sustainability policies to reduce greenhouse emissions, [90]. The total capacity of wind energy installed in Europe by the end of 2009 was about $76GW$, [91]. This amount is predicted to be about $180GW$ with $35GW$ offshore, and $300GW$ with $120GW$ offshore for 2020 and 2030, respectively, [92]. Therefore, such wind farm connections have become the main attention point of most countries which potentially have the capability of wind power generation.

However, uncertainty associated with these non-dispatchable sources has brought several challenges to power system planning, operation, and control, [93]. This un-

certainty can cause additional operating costs for energy procurement. This also causes major challenges for power systems operation and planning.

Several papers have studied the impact of wind power integration on various power system aspects, [94–101]. There are several barriers and technical constraints limiting the level of wind power integration (such as transmission congestion, local network constraints, minimum operating levels of thermal generators and system stability limits such as voltage problems, [102]). Among the constraints imposed by stability criteria, the voltage stability is one important factor in limiting wind power penetration into the power system, [103]. In this chapter, we deal with Voltage Stability Margin (VSM) for improving the wind power integration in power systems. We propose an optimization model to cope with this issue. Increase in the wind power level can lead to greater demand of reactive power. If the reactive power demand is not met by either wind power plant or the power system to which wind turbine is connected, it may result in voltage stability issues, [53, 103–108].

Voltage stability issue is a more highlighted problem in wind farms with Fixed-Speed Wind Turbines (FSWTs) which require reactive power support from the grid. Contrary to FSWTs, variable-speed turbines such as Doubly Fed Induction Generators (DFIG) are capable of providing reactive power to the grid. Yet the impact of reactive power output of DFIG-based wind turbines on the voltage profile and stability of power systems has been the main concern in literature, [98, 109–111]. Several studies have investigated different aspects of voltage stability problems associated with wind power generation. Reference [112] studies the feasibility of utilizing the reactive power of grid-connected variable-speed wind generators to enhance the steady-state voltage stability margin of the system. Modal analysis and traditional voltage stability methods (Q-V curves) have been adopted in reference [108] to increase wind penetration levels by allocating SVCs. Reference [111] evaluates the impact of wind generation on the voltage stability of a power system using time-series and AC power flow analysis. This reference has shown how the voltage stability margin of the power system can be increased through the proper implementation of voltage control strategies in wind turbines. The probabilistic risk of voltage collapse caused by intermittent nature of renewable energy sources is the main focus in reference [113]. To lower the computational burden, authors in [114] have applied a Stochastic Response Surface Method (SRSM) to analyze the impact of uncertain power injections including wind generation on the load margin which is directly connected to voltage collapse point.

In all of these studies, the wind farms are assumed to be located close and directly connected to the main AC grid using conventional AC connection. However, the AC connection of large wind farms located more than ten kilometers far from the main AC grids brings up several challenges for power system operators, [115–117]. The VSC based HVDC transmission technology has been identified as a superior alternative for integrating far-located large wind farms, [115, 118–120], especially through a multi-terminal HVDC system to the main AC grid, [120]. To the best of authors' knowledge, there is no work on voltage stability assessment considering maximization of wind power from VSC-DC grid connected wind farms.

This chapter proposes a conic OPF with voltage stability constraint of AC grid and VSC-based multi-terminal DC grids. This model will be used to study the impact of wind power connected to the DC grid on voltage stability of AC grid. This is done by modifying perviously proposed CAD-OPF model to ensure a certain voltage stability margin for wind power integration. The objective of the proposed optimization model is to maximize the wind power injection to the grid by optimal tuning of installed VSC-HVDC links connecting wind farms to the grid. The maximization of wind power penetration is done by minimizing wind power curtailment which might be required to mitigate the impact of the deviation between forecasted and realized wind power outputs.

6.3 Motivation of Proposed Model

Since wind energy is cheap and green, it is desirable to absorb as much as possible of the available wind power, as long as the network constraints are met. However, there are some cases where system operator prefers to use a smaller amount of available wind power due to transmission or stability constraints, [102]. Accepting less wind power than its available amount is called wind power curtailment.

Several reasons such as transmission congestion, local network constraints, minimum operating levels of thermal generators, and system stability limits including voltage problems may lead to the wind power curtailment. Wind power curtailment can also be adopted as a solution for critical conditions where wind power is above its maximum limit, [103]. The cost of curtailment, which is carried by the Transmission System Operator (TSO), has become an incentive for several TSOs and regulators such as Italian regulator to reduce the amount of curtailments, [102]. The Delivering A Secure Sustainable Electricity System Program proposes various plant performance monitoring and new ancillary services to reduce the level of curtailment, [121].

Ensuring Voltage Stability Margin (VSM) can be also a reason for wind power curtailment. It is possible to calculate VSM at different operating points with a high degree of certainty when generator outputs are certain. However, in case of presence of some uncertain energy sources such as wind generators, it is more complicated to assess the VSM before realization of wind generator outputs. Therefore if one assesses the VSM for wind-integrated systems considering predicted wind powers, it might results in miscalculation of VSM for realized wind powers during the real-time operation of system.

Ignoring the deviation of the realized wind power outputs from forecasted ones might drive the system to an operating point close to voltage stability collapse point. This may endanger the system if a disturbance occurs while a risky level of wind power is realized. Therefore, it is beneficial to check the voltage stability constraint close to real-time when the wind power output has the maximum forecast error.

To do this, we propose an OPF model incorporating both AC and DC grids and VSC links where it is solved close to real-time to minimize the wind power curtailment while ensuring a certain VSM for all realized wind power scenarios. We take advantage of the fast and flexible operation of VSC converters especially their capability of injecting/absorving reactive power at the point of connection to the grid which makes them perfectly suitable to cope with the deviations of wind power production.

Through the proposed OPF model, optimal settings of VSC converters are determined in such a way that for each realized wind power scenario, the wind curtailment, if needed, is minimized while ensuring a certain VSM per wind scenario. Second priority is to minimize network transmission losses. Different control modes for converters are taken into account and associated results are presented and discussed.

6.4 Framework

In the framework considered in this chapter, we assume that the "day-ahead market" is cleared with forecasted or averaged wind power outputs for each hour of operation. This means that hourly schedule for active power productions and demands are determined for the coming day in this market. Outputs of this market are used as inputs of our proposed OPF model. The outputs of the day ahead market are indicated with fix index. While the rest of variables depend on wind power scenarios (s).

While the time framework for day-ahead market is 24 hours, the time framework for VSM assessment proposed in this chapter is 1 hour. This means that the proposed optimization model is to run hour by hour, [122]. We assume that system operator runs the proposed OPF model close enough to each hour of the system operation while the latest wind power forecasts are available. We also assume that prior to each hour of operation, wind power uncertainty is modeled as a set of scenarios. The OPF model is then solved for a set of scenarios corresponding to updated wind power outputs per hour. This way, the system operator will form a look-up table containing optimal settings of HVDC links required for any plausible scenario of wind power where the wind power curtailment is minimized while a given voltage stability margin is assured. Therefore, if any of these scenarios is realized its corresponding optimal settings are available to be set.

6.5 The Voltage Stability Constrained CAD-OPF model

In this section the proposed Voltage Stability Constrained CAD-OPF (VSC-CAD OPF) model is presented. In perviously presented models, the nonlinear set

of AC power flow equations are recast as a convex set using exact relaxations and two well-known approximations (i.e. $sin(\Delta\theta) \approx \Delta\theta$ and $V_{se}V_r \approx 1$). In this chapter, however, to capture more accurate results especially associated with voltage magnitudes, Taylor Series is used to derive the phase angle constraints. It should be noted that for better accuracy, an extra iterative loop is added to the pervious models. However, the whole model is still convex and can be efficiently solved. The objective function of proposed VSCCAD-OPF model is selected as follow:

$$Minimize \sum_{s\in S}\pi_s[\sum_{\omega\in\Upsilon}\alpha_\omega(P^s_{\omega,ci})+\sum_{l\in N_l}\alpha_l(P^s_{lossl})+\sum_{l\in N_l^{dc}}\alpha_{ldc}(P^s_{dlossl})] \tag{6.1}$$

The first term in (6.1) is total wind power curtailment while the second term is active power losses in both AC and DC grids. The minimization of active power loss is in the second priority. It should be highlighted that the load shedding also might be considered in the objective. The importance of each term is specified by three weighting factors given in (6.1). To incorporate the voltage stability margin, we use the loading margin λ. The objective function in (6.1) is subjected to a set of constraints listed as:

Current Loading Conditions

AC Network Constraints:

$(\forall i \in N_b,\ \forall s \in S,\ \forall l \in N_l, W = V^2)$

$$P^s_{gi} - P_{di} + P^s_{Ci} + (P^s_{\omega i} - P^{fix}_{\omega i} - P^s_{\omega,ci}) = \sum_{l=1}^{N_l}\boldsymbol{M_{PQ}}(i,l)P^s_{rl} + \sum_{l=1}^{N_l}\boldsymbol{M_{loss}}(i,l)P^s_{lossl} \tag{6.2}$$

$$Q^s_{gi} - Q_{di} + Q^s_{Ci} = \sum_{l=1}^{N_l}\boldsymbol{M_{PQ}}(i,l)Q^s_{rl} + \sum_{l=1}^{N_l}\boldsymbol{M_{loss}}(i,l)Q^s_{lossl} - B_i W^s_i \tag{6.3}$$

$$W^s_{sel} - W^s_{rl} = 2R_l P^s_{rl} + 2X_l Q^s_{rl} + R_l P^s_{lossl} + X_l Q^s_{lossl} \tag{6.4}$$

$$2\beta^s_{lossl} W^s_{rl} \geq (P^s_{rl})^2 + (Q^s_{rl})^2 \tag{6.5}$$

$$X_l P^s_{lossl} - R_l Q^s_{lossl} = 0 \tag{6.6}$$

where wind power scenarios are represented by index s. S is the set of wind power scenarios. Constraints (6.2) and (6.3) are active/reactive power mismatch equations. In (6.2), active power production of each generating unit is considered as follows:

$$P_{gi}^{s} = P_{gi}^{fix} + \Delta P_{gui}^{s} - \Delta P_{gdi}^{s} \tag{6.7}$$

where P_{gi}^{fix} is dispatched power in the market. The ΔP_{gui} and ΔP_{gdi} are increment and decrement in generators outputs. In order to incorporate phase angle constraints we use following expression associated with voltage drop across each AC line.

$$V_{sel}e^{j\theta_{sel}} = V_{rl}e^{j\theta_{rl}} + \frac{P_{rl} - jQ_{rl}}{V_{rl}e^{-j\theta_{rl}}}(R_l + jX_l) \tag{6.8}$$

One can obtain the imaginary and real parts of equation (6.8):

$$V_{sel}^{s}V_{rl}^{s}\sin(\theta_{sel}^{s} - \theta_{rl}^{s}) = X_l P_{rl}^{s} - R_l Q_{rl}^{s} \tag{6.9}$$

$$V_{sel}^{s}V_{rl}^{s}\cos(\theta_{sel}^{s} - \theta_{rl}^{s}) = R_l P_{rl}^{s} + X_l Q_{rl}^{s} + (V_{rl}^{s})^2 \tag{6.10}$$

Dividing (6.9) by (6.10) gives us the following expression for phase angle difference across each line ($(V_{rl}^{s})^2 = W_{rl}^{s}$) :

$$\theta_{sel}^{s} - \theta_{rl}^{s} = \tan^{-1}\left(\frac{X_l P_{rl}^{s} - R_l Q_{rl}^{s}}{R_l P_{rl}^{s} + X_l Q_{rl}^{s} + W_{rl}^{s}}\right) \tag{6.11}$$

Lets define two new variables as $H = X_l P_{rl}^{s} - R_l Q_{rl}^{s}$ and $A = R_l P_{rl}^{s} + X_l Q_{rl}^{s} + (V_{rl}^{s})^2$. To include the nonlinear expression (6.11) into the proposed conic OPF, we use Taylor Series expansion around an initial estimate (H^o, A^o) and neglect higher order terms as follows:

$$\theta_{sel}^{s} - \theta_{rl}^{s} = \tan^{-1}\left[\frac{H^o}{(A^o)^2}\right] + \frac{H^o}{(H^o)^2 + (A^o)^2}H - \frac{A^o}{(H^o)^2 + (A^o)^2}A \tag{6.12}$$

DC Network Constraints:

$$(\forall i \in N_b^{dc},\ \forall s \in S,\ \forall l \in N_l^{dc}, W_{dc} = V_{dc}^2)$$

$$P_{dc,i}^{s} = -\sum_{l=1}^{N_l^{dc}} \boldsymbol{M_{P_{dc}}}(i,l)P_{dc,rl}^{s} - \sum_{l=1}^{N_l^{dc}} \boldsymbol{M_{loss,dc}}(i,l)P_{dlossl}^{s} \tag{6.13}$$

$$W_{dc,sel}^{s} - W_{dc,rl}^{s} = (2P_{dc,rl}^{s} + P_{dlossl}^{s})R_{dc,l} \tag{6.14}$$

$$2\beta^s_{dlossl} W^s_{dc,rl} \geq (P^s_{dc,rl})^2 \tag{6.15}$$

VSC Converter Constraints:

$$\begin{aligned}&(\forall i \in N^{dc}_b,\ \forall s \in S,\ \forall l \in N^{dc}_l)\\ &8W^s_{pc,i} - m^2_{C,M} W^s_{dc,i} \leq 0\end{aligned} \tag{6.16}$$

$$m^2_{C,m} W^s_{dc,i} - 8W^s_{pc,i} \leq 0 \tag{6.17}$$

$$P^s_{lshi} R_{Csh} = W^s_{dc,i} \tag{6.18}$$

$$P^s_{Ci} = P^s_{dc,i} - P^s_{lshi} \tag{6.19}$$

OPF model

Now we set out the proposed convex optimization model. To incorporate voltage stability constraint, we consider a loading margin λ which represents a critical loading condition (variables indexed by $\hat{x}$) larger than the normal one, [122]. The proposed VSCCAD-OPF model is given as follows:

$$\textit{Minimize} \sum_{s\in S} \pi_s [\sum_{\omega \in \Upsilon} \alpha_\omega(P^s_{\omega,ci}) + \sum_{l \in N_l} \alpha_l(P^s_{lossl}) + \sum_{l \in N^{dc}_l} \alpha_{ldc}(P^s_{dlossl})] \tag{6.20}$$

Subject to:
Constraints associated with normal loading condition:
(6.2), (6.3), (6.4), (6.5), (6.6), (6.12), (6.13), (6.14), (6.15), (6.16), (6.17), (6.18), (6.19)

Constraints associated with security loading condition:

$$\begin{aligned}&\forall i \in N_b,\ \forall s \in S,\ \forall l \in N_l,\ W = V^2\\ &\hat{P}^s_{gi} - \hat{P}_{di} + \hat{P}^s_{Ci} + (P^s_{\omega i} - P^{fix}_{\omega i} - P^s_{\omega,ci}) = \sum_{l=1}^{N_L} \boldsymbol{M_{PQ}}(i,l)\hat{P}^s_{rl} + \sum_{l=1}^{N_L} \boldsymbol{M_l}(i,l)\hat{P}^s_{lossl}\end{aligned} \tag{6.21}$$

$$\hat{Q}^s_{gi} - \hat{Q}_{di} + \hat{Q}^s_{Ci} = \sum_{l=1}^{N_L} \boldsymbol{M_{PQ}}(i,l)\hat{Q}^s_{rl} + \sum_{l=1}^{N_L} \boldsymbol{M_l}(i,l)\hat{Q}^s_{lossl} - B_i \hat{W}^s_i \tag{6.22}$$

$$\hat{W}^s_{sel} - \hat{W}^s_{rl} = 2R_l\hat{P}^s_{rl} + 2X_l\hat{Q}^s_{rl} + R_l\hat{P}^s_{lossl} + X_l\hat{Q}^s_{lossl}) \tag{6.23}$$

$$2\hat{\beta}^s_{lossl}\hat{W}^s_{rl} \geq (\hat{P}^s_{rl})^2 + (\hat{Q}^s_{rl})^2 \tag{6.24}$$

$$X_l\hat{P}^s_{lossl} - R_l\hat{Q}^s_{lossl} = 0 \tag{6.25}$$

$$\hat{\theta}^s_{sel} - \hat{\theta}^s_{rl} = \tan^{-1}\left[\frac{H^o}{(A^o)^2}\right] + \frac{H^o}{(H^o)^2 + (A^o)^2}\hat{H} - \frac{A^o}{(H^o)^2 + (A^o)^2}\hat{A} \tag{6.26}$$

$$\hat{P}^s_{gi} = (1 + \lambda^s + K_{gi})P^s_{gi} \tag{6.27}$$

$$\hat{P}_{di} = (1 + \lambda^s)P_{di} \tag{6.28}$$

$$\hat{Q}_{di} = (1 + \lambda^s)Q_{di} \tag{6.29}$$

$$W^m_i \leq \hat{W}^s_i, W^s_i \leq W^M_i \tag{6.30}$$

$$P^m_{gi} \leq \hat{P}^s_{gi}, P^s_{gi} \leq P^M_{gi} \tag{6.31}$$

$$Q^m_{gi} \leq \hat{Q}^s_{gi}, Q^s_{gi}, \leq Q^M_{gi} \tag{6.32}$$

$$\Delta P^m_{gui} \leq \Delta P^s_{gui} \leq \Delta P^M_{gui} \tag{6.33}$$

$$\Delta P^m_{gdi} \leq \Delta P^s_{gdi} \leq \Delta P^M_{gdi} \tag{6.34}$$

$$\lambda^s = \lambda_{des} \geq 0 \tag{6.35}$$

$$0 \leq P^s_{\omega,ci} \leq P^s_{\omega i} - P^{fix}_{\omega i} \tag{6.36}$$

$$\forall i \in N^{dc}_b,\ \forall s \in S,\ \forall l \in N^{dc}_l,\ \hat{W}_{dc} = \hat{V}^2_{dc},\ \hat{W}_{pc} = \hat{V}^2_{pc}$$

$$\hat{P}^s_{dc,i} = -\sum_{l=1}^{N^{dc}_L} \boldsymbol{M_{P_{dc}}}(i,l)\hat{P}^s_{dc,rl} - \sum_{l=1}^{N^{dc}_L} \boldsymbol{M_{l_{dc}}}(i,l)\hat{P}^s_{dlossl} \tag{6.37}$$

$$\hat{W}^s_{dc,sel} - \hat{W}^s_{dc,rl} = (2\hat{P}^s_{dc,rl} + \hat{P}^s_{dlossl})R_{dc,l} \tag{6.38}$$

$$2\hat{\beta}^s_{dlossl}\hat{W}^s_{dc,rl} \geq (\hat{P}^s_{dc,rl})^2 \tag{6.39}$$

$$8\hat{W}^s_{pc,i} - m^2_{C,M}\hat{W}^s_{dc,i} \leq 0 \tag{6.40}$$

$$m^2_{C,m}\hat{W}^s_{dc,i} - 8\hat{W}^s_{pc,i} \leq 0 \tag{6.41}$$

$$\hat{P}^s_{lshi}R_{Csh} = \hat{W}^s_{dc,i} \tag{6.42}$$

$$\hat{P}^s_{Ci} = \hat{P}^s_{dc,i} - \hat{P}^s_{lshi} \tag{6.43}$$

$$(P^s_{Ci})^2 + (Q^s_{Ci})^2 \leq CAP^2_{Ci} \tag{6.44}$$

$$(\hat{P}^s_{Ci})^2 + (\hat{Q}^s_{Ci})^2 \leq CAP^2_{Ci} \tag{6.45}$$

$$W^m_{dc,i} \leq \hat{W}^s_{dc,i}, W^s_{dc,i} \leq W^M_{dc,i} \tag{6.46}$$

Note that through this optimization model unexpected deviations of wind power violating voltage stability margin are corrected with wind power curtailment and/or active power decrement/increment in generation units.

6.6 Wind Uncertainty Modelling

Several approaches have been proposed for wind uncertainty modeling. One approach is accurate prediction of wind power through advanced forecasting techniques, [123]. Another approach is based on designing stochastic processes, [124]. In this approach, variable wind power is represented by a set of finite scenarios with corresponding probability of occurrence. To generate scenarios different methods such as path based methods, movement matching and internal sampling have been proposed, [125, 126]. Rayleigh PDF widely used to model the behavior of wind, [127]. Rayleigh PDF is a special form of Weibull PDF in (6.47) with shape factor $k = 2$.

$$f(v \mid k, c) = (\frac{k}{c})(\frac{v}{c})^{(k-1)} exp[-(\frac{v}{c})^k] \tag{6.47}$$

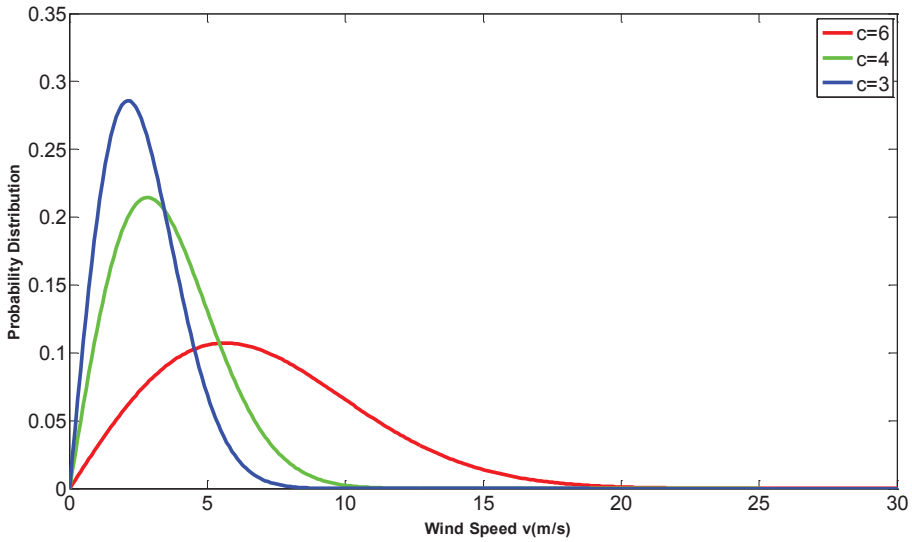

Figure 6.1: Rayleigh PDF with three different scale factors.

In expression (6.47), c is the scale factor at a given location for each wind power unit. Figure 6.1 shows Rayleigh PDFs with three different scale factors. The output power scenarios are to be calculated through speed-power relation curve. This curve is obtained through a set of experimental values from manufacturer. In the literature different mathematical expressions have been proposed for this curve. A linear approximation of this curve is as follows, [128]:

$$P_\omega = \begin{cases} 0 & \text{if } v_s < v_{in} \text{ or } v_s > v_{out} \\ P_{\omega r} & \text{if } v_r < v_s < v_{out} \\ (\frac{v_s - v_{in}}{v_r - v_{in}}) P_{wr} & \text{if } v_{in} < v_s < v_r \end{cases} \tag{6.48}$$

where v_{in}, v_{out} and v_r are cut-in, cut-out and rated wind speed, respectively. P_W and P_{wr} are power output and rated power of wind turbine, respectively. In this thesis, for the sake of simplicity, we assume a set of wind power scenarios are available to be used as inputs to the proposed model.

6.7 Case Study and Simulation Results

To evaluate the proposed optimization model a modified version of IEEE 30-bus [67] test system is used. Three wind farms WF1, WF2 and WF3 are connected to buses 13, 14 and 15, respectively (See Figure 6.3).

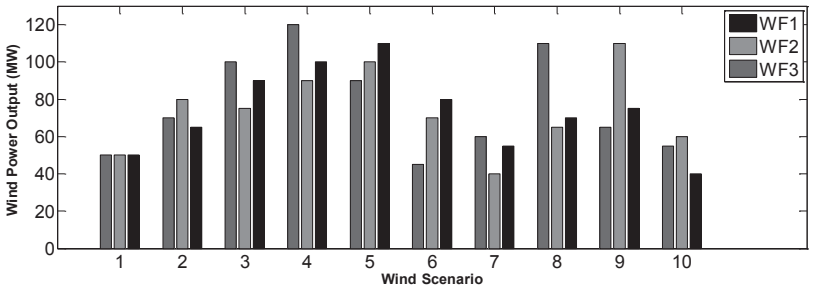

Figure 6.2: Wind power scenarios associated to wind farm outputs .

The dispatched power of wind farms considered in the market are assumed to be 20, 30 and 40 MW, respectively. The uncertainty of the wind power outputs are modeled through 10 wind power scenarios shown in Table 6.2. For the simplicity, the probabilities of all scenarios (π_s) are assumed to be identical and equal to 0.1. Generation outputs for G1, G2, G5, G8 and G11 scheduled in day-ahead market are 103.76, 34.77, 13.18, 19.63 and 22.06, respectively. The maximum increment/decrement of generation outputs are considered equal to $50MW$ for all units. The minimum and maximum value of modulation index m_C is assumed to be 0.5 and 1, respectively. Minimum and maximum values for AC voltage buses are qual to 0.94 and 1.06 p.u. The limits of DC bus voltages are obtained based on the limits of AC voltage buses. The resistance of DC lines are assumed to be equal to 0.01 p.u.

In order to study the impact of wind penetration on the connected AC grid we modified the reactance of lines close to wind farms connection point. Reactance of lines (4,12), (12,13), (12,15), (12,16), (23,24) and (18,19) are set to 0.3,0.11, 0.2304, 0.2987, 0.17 and 0.1 p.u. Different cases considered in this section are:

Table 6.1: Comparison between results obtained from Cases A, B and C

	$\mathbf{E}[\Sigma P_{\omega,c}](MW)$	λ_{max}
Case A	0	0.28
Case B	70.99	0.37
Case C	61.87	0.37
Percentage of reduction in wind power curtailment (%)	12	

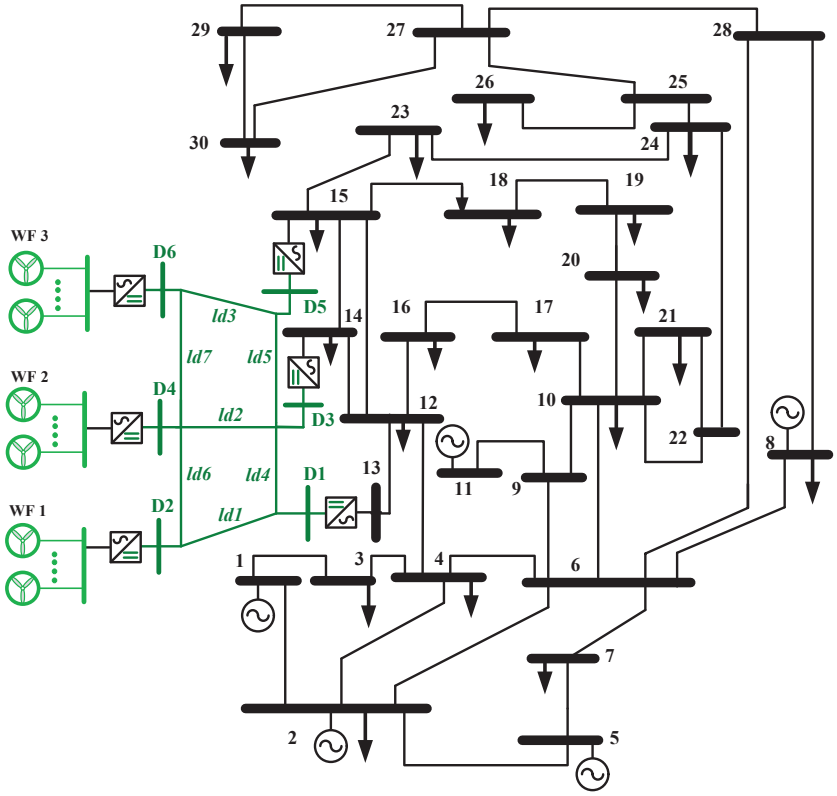

Figure 6.3: Modified IEEE 30-Bus test system with three connected wind farms .

Case A) All wind farms are connected directly to the AC buses and no wind power curtailment is allowed.
Case B) All wind farms are connected directly to the AC buses and wind power curtailment is allowed.
Case C) All wind farms are connected directly to the AC buses and wind power curtailment is allowed and minimized.
Case D) All wind farms are connected through VSC-DC grid shown in Figure 6.3 to the AC grid and wind power curtailment is allowed.
Case E) All wind farms are connected through VSC-DC grid shown in Figure 6.3 to the AC grid and wind power curtailment is allowed and minimized.

Impact of loading margin on amount of wind power curtailment without VSC-DC grid

The comparison between results obtained from Case A, B and C are reported in Table 6.1. From the results, it is obvious that when no wind power curtailment is allowed a smaller maximum loading margin can be achieved. It can be also concluded from the results that the percentage of reduction in wind power curtailment in Case C compared to Case B is 12%. This reduction in wind power curtailment has been achieved while the maximum loading margin is identical for both Cases and is $\lambda_{max,BC} = \mathbf{0.37}$.

Table 6.2: Comparison between results obtained from Cases D and E

Loading Margin (λ)	$\lambda_1 = 1.60$	$\lambda_2 = 1.65$	$\lambda_3 = 1.70$	$\lambda_4 = 1.75$
$\mathbf{E}[\Sigma P_{\omega,c}](MW)$ Case D	73.59	82.37	97.59	116.80
$\mathbf{E}[\Sigma P_{\omega,c}](MW)$ Case E	30.79	48.63	67.47	86.10
Percentage of reduction (%)	58	41	30.8	26.2

Impact of loading margin on amount of wind power curtailment with VSC-DC grid

In another analysis, we study two cases where the wind farms are connected to the AC grid through a VSC-DC grid (See Figure 6.3). In Case D for all wind power scenarios wind power curtailment is allowed while in Case E the wind power curtailment is allowed but minimized. The maximum loading margin achieved in Cases D and E is equal to $\lambda_{max,DE} = \mathbf{0.8}$. The results for four different loading margins for these two cases are given in Table 6.2.

The first conclusion from comparing the results in Table 6.2 and Table 6.1 is that in Case E where the wind farms are connected through VSC-DC grid and the wind power curtailment is minimized, it is possible to have smaller curtailed wind power with a higher loading margin compared to Case C where the wind farms are directly connected to the AC grid. The second conclusion from obtained results for Cases D and E is that ensuring a higher loading margin leads to a lower percentage of wind power curtailment.

Optimal settings of VSC converters to minimize curtailed wind power while ensuring a certain loading margin

To show how settings of converters are optimally tuned in order to maximize the absorbed wind power to the grid while a certain loading margin is ensured two cases D and E are used for a certain loading margin of $\lambda = 1.73$. In Case D, the objective is to minimize the losses while loading margin $\lambda = 1.73$ is ensured. However, in Case E, the main objective is to minimize the curtailed wind power and at the same time the same loading margin as considered in Case D is to be ensured. It should be noted that minimization of transmission losses in this case is the second priority. This gives us a curtailed wind power of **98.50 MW** in Case D and **65.83 MW** in Case E which corresponds to **33.16%** reduction in the curtailed wind power.

Figure 6.4 illustrates how reactive power of converters are determined to achieve a certain loading margin ($\lambda = 1.73$) and a minimum wind power curtailment. The corresponding values for the injected/absorbed active power at DC buses are shown in Figure 6.5. The negative value indicates that the direction of the power flow is from converter to the DC bus and positive value indicates that the direction of the power flow is from the DC bus towards the VSC station. It is seen that in case E where the main objective is to minimize curtailed wind power a larger level of DC power from wind farm side is transferred through the VSC-DC grid to the main AC grid.

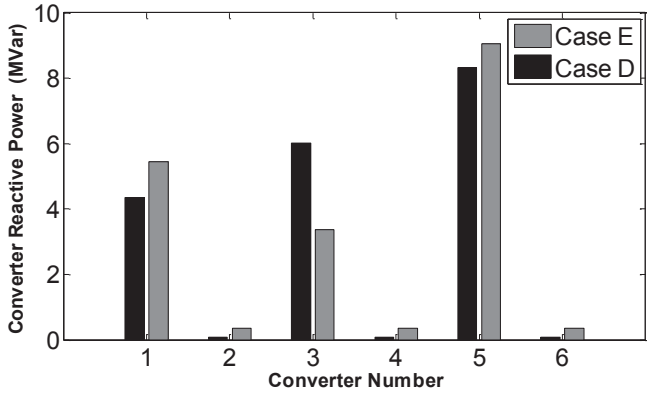

Figure 6.4: The reactive power setting of VSC converters for wind scenario 2 .

The optimal modulation indices of VSC converters (m_C) in Case E corresponding to different loading margins λ which have been determined through the proposed model in Case E are reported in Table 6.3. It can be observed from these results that for each desirable loading margin a set of optimal parameters for VSC links

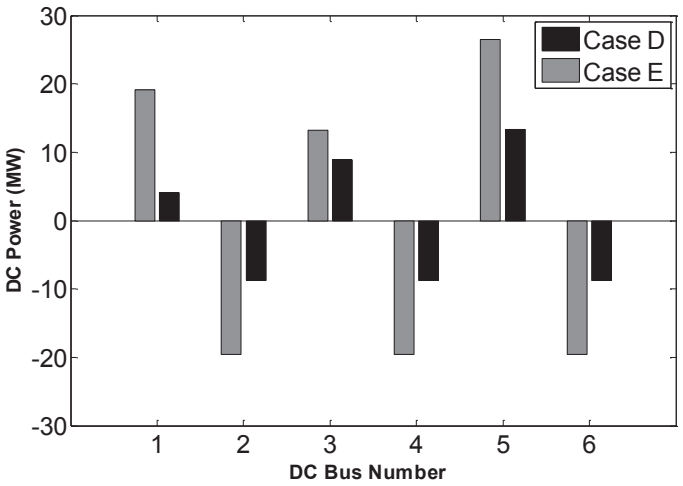

Figure 6.5: Active power at each DC bus for wind scenario 2 .

Table 6.3: Optimal modulation indices of VSC converters in Case E for different values of loading margin λ

	m_{C1}	m_{C2}	m_{C3}	m_{C4}	m_{C5}	m_{C6}
$\lambda = 0.62$	0.63008	0.60952	0.56375	0.60953	0.59559	0.60974
$\lambda = 0.68$	0.62833	0.61009	0.56521	0.61009	0.59388	0.61010
$\lambda = 0.69$	0.71847	0.69773	0.64709	0.69773	0.67899	0.69774
$\lambda = 0.70$	0.85272	0.82828	0.76871	0.82828	0.80595	0.82830
$\lambda = 0.71$	0.97047	0.94295	0.87558	0.94295	0.91739	0.94297
$\lambda = 0.72$	0.99997	0.97204	0.90301	0.97204	0.94541	0.97206

should be determined leading to a maximum wind power integration into the grid. These optimal settings can be set for VSC converters when the corresponded wind scenario is realized in the real time. It should be highlighted that the computational time in all simulations in this section is less than **1.5 second**. This makes the proposed model very suitable for the real-time application where a fast solution is desired.

Both minimized real transmission loss and curtailed wind power obtained from the proposed model are illustrated in Figure 6.6. It is observed that a higher desirable loading margin needs a higher level of wind power curtailment. It is also observed that a higher level of wind power curtailment results in a lower minimized active transmission loss.

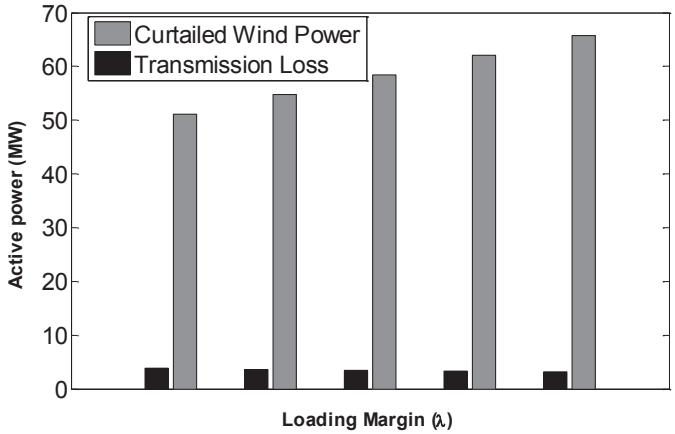

Figure 6.6: Active power at each DC bus for wind scenario 2 .

Part IV

Closure

Chapter 7

Conclusion and Future Work

7.1 Conclusion

This chapter provides conclusions drawn from this thesis. In this thesis as a response to a need for more efficient and more accurate Power Flow Scheduling and Balancing models, two main analysis tools which are used in power scheduling, balancing and system operation i.e. Power Flow (PF) and Optimal Power Flow (OPF) models are studied. Due to nonlinear and non-convex nature of power flow equations it is hard to achieve both efficiency and accuracy from existing solution approaches. This is why researchers have divided the solution approaches into two main groups i.e. Nonlinear Programming (NLP) and Linear Programming (LP).

Through NLP approaches, the nonlinearity of the power system is fully represented for the sake of accuracy but with the cost of complexity in the models. The computational and theoretical challenges associated with NLP approaches are then used as a motivation towards developing a more simplified power flow formulation, which led to the second group of LP models. In LP models, the nonlinearity and non-convexity of the full AC power flow model are completely removed from the problem through both simplifying assumptions (DC-OPF) and linearization techniques such as Sequential Linear Programming (SLP). Because of convexity of the LP approaches it is possible to efficiently handle constraints and quickly recognize problem infeasibility and also guarantee a global optimal solution. However, the obtained global optimum is not the global optimum to the original nonlinear and non-convex AC-OPF problems. Moreover, the LP approaches suffer from the lack of accuracy in the results. According to the mentioned advantages and disadvantages of NLP and LP based OPFs, in this thesis we propose an OPF model which benefits from main advantages of both approximated OPF models (Efficient numerical solvers) and full AC OPF models (Results accuracy).

The thesis is divided into two main parts: AC networks analysis and AC-DC networks analysis without and with wind power integration. To study these two

parts, this thesis proposes a conic format of conventional power flow equations. The derived conic format is a convex optimization problem. This is achieved through reformulation and convexification of nonlinear and non-convex power flow equations using three techniques: change of variables, relaxation, and approximation. The conclusions drawn from this thesis are listed in order.

- **AC Power Flow Problem as a Convex Optimization Problem:** This thesis proposes a convex optimization problem as a solution tool for AC-PF problems in a more robust and efficient way. The proposed conic PF (CPF) model is derived for radial networks through reformulation of conventional AC power flow equations and applying an exact relaxation. State variables in the proposed optimization problem consists of bus voltages, active and reactive power flows and losses of lines which reflect more practical knowledge of the system. The obtained set of equations are then used as constraints of an optimization problem where the choice of objective function makes the proposed relaxation exact. The proposed optimization problem is exactly in the form of conic optimization which is a convex problem and can be efficiently solved through Interior Point Methods (IPMs). The proposed conic optimization problem can efficiently and robustly handle both well- and ill-conditioned radial networks. Since there is no approximation in the model the results are identical to results obtained from other approaches.

  In the next step, this thesis proposes a very good approximation to extend the proposed CPF to be used as a solution tool for meshed AC networks. Using proposed approximations and graph theory, nonlinear set of equations associated with phase angle constraints becomes linear and well-suited to be incorporated into the CPF model. The extended CPF (ECPF) can efficiently and robustly handle both well- and ill-conditioned meshed networks. Although the approximation used in the ECPF model affects the accuracy of results, the output of ECPF is very close to results from other approaches.

- **Conic AC Optimal Power Flow Model and Negative LMPs:** In another study, the proposed ECPF model is used to solve an AC-OPF where the objective is to minimize generation costs. Since the quadratic generation cost function is not consistent with conic format, this thesis proposes a conic format of quadratic cost function. The proposed Conic AC-OPF (CAC-OPF) model is a convex problem. According to literature and obtained numerical results in this thesis, the relaxed inequalities used in the proposed CAC-OPF are always binding at the optimality provided that the objective function is convex and Locational Marginal Prices (LMPs) at all system buses are positive.

  The impact of emerging negative LMPs on the relaxed conic optimization is also studied. This issue can stem from emerging a gap between two sides of the relaxed inequality as a result of negative LMPs. We show that negative LMPs, which might be miscalculated through other conic and semidefinite

problems, can be correctly emerged in the output of the proposed CAC-OPF model. This is done by adding a linear term into the objective function with a penalty factor.

- **Convexified AC-DC Optimal Power Flow Model in Conic Format:** Followed by pervious studies in this thesis, the proposed conic format of power flow equations are used to develop a Conic AC-DC OPF (CAD-OPF) model which can be applied to hybrid AC-DC grids incorporating VSC-DC grids and shunt FACTS devices. These devices can bring several benefits to the power systems. However, before identifying their benefits, they need to be properly included in the optimization model. In order to incorporate them into the conic optimization problem, all constraints associated to these devices were transformed into the conic format. Through proposed CAD-OPF, it is possible to optimize several objectives by optimal tuning of parameters of these flexible devices.

- **Maximization of Wind Power Penetration Ensuring a Certain Voltage Stability Margin:** Finally, as an application of CAD-OPF, a voltage stability constrained version of CAD-OPF (VSCCAD-OPF) is proposed. The proposed VSCCAD-OPF model is to analyze one of the existing challenges which power systems experience as a result of intermittent nature of wind power output. This is done by modifying perviously proposed CAD-OPF model to ensure a certain voltage stability margin in the real-time operation of power systems. The objective of the proposed optimization is to maximize the wind power injection to the grid by optimal tuning of installed VSC-HVDC links connecting wind farms to the grid. First of all, it is shown that if a system operator is to ensure a certain Voltage Stability Margin (VSM) for any realization of wind power scenarios, it might require some wind power curtailment. This wind power curtailment increases by increasing VSMs. It is also shown that if the wind farms are directly connected to the main AC grid, the Maximum Achievable Voltage Stability Margin (MAVSM) is considerably smaller than MAVSM of the cases where wind farms are connected to the main AC grid through VSC-DC grids. It should be highlighted that the amount of wind power curtailment in case of VSC-DC grid integrated wind farms are lower than the case where the wind farms are directly connected to the grid. This is obtained through proposed VSCCAD-OPF where VSC-DC grid's parameters are optimally determined in such a way that it achieves a larger VSM with a lower wind power curtailment.

7.2 Future Work

The proposed convex models i.e. CPF, ECPF, CAC-OPF, CAD-OPF and VSCCAD-OPF can be adopted as analytical tools for different studies such as power flow scheduling, power balancing, power system operation, power system planning, transmission switching. Some extensions to this thesis are:

- **Power system flexibility** : The wind power integration introduces an increasing level of uncertainty in electricity markets modeling and design problems. The wind power uncertainty can be properly handled by improving the system flexibility by efficient operation of and investment in flexibility resources. A flexibility resource is capable of ramping its output upwards or downwards in response to a sudden change in wind power production. The system operator employs its system ramping capability to handle a credible change in the wind power output. The proposed PF and OPF models in this thesis can be extended to incorporate ramping capability. Through this ramp-rate constrained models it is possible to measure how flexible the system is to recover from a contingency or a sudden change such as changes in wind power outputs.

- **Impact of MTDC systems on the power system recovery from contingencies**: As an another extension of this work, one can study the impact of VSC-DC grids and FACTS devices on the power system recovery from possible contingencies.

- **Embedding convex optimization problems in dynamic analysis of MTDC systems to handle wind power variability in a more optimal and efficient way**: Since convex optimization models in this thesis are efficient and fast to be solved, they can be used for dynamic analysis of power systems. As an example, dynamic analysis of MTDC grids with wind farms can be performed using the proposed conic OPFs in this work.

Bibliography

[1] "Smart grid concept and characteristics." [Online]. Available: http://electrical-engineering-portal.com/smart-grid-concept-and-characteristics

[2] "Midwestiso, lmp contour map from 2:40 pm, june 22, 2011." [Online]. Available: http://www.midwestmarket.org

[3] B. Lesieutre, D. Molzahn, A. Borden, and C. DeMarco, "Examining the limits of the application of semidefinite programming to power flow problems," in *Communication, Control, and Computing (Allerton), 2011 49th Annual Allerton Conference on*, 2011, pp. 1492–1499.

[4] S. Tripathy, G. Prasad, O. P. Malik, and G. Hope, "Load-flow solutions for ill-conditioned power systems by a newton-like method," *Power Apparatus and Systems, IEEE Transactions on*, vol. PAS-101, no. 10, pp. 3648–3657, Oct 1982.

[5] R. Piwko, P. Meibom, H. Holttinen, B. Shi, N. Miller, Y. Chi, and W. Wang, "Penetrating insights: Lessons learned from large-scale wind power integration," *Power and Energy Magazine, IEEE*, vol. 10, no. 2, pp. 44–52, March 2012.

[6] "Iea technology roadmap: Wind energy," 2013.

[7] E. Lannoye, D. Flynn, and M. O'Malley, "Evaluation of power system flexibility," *Power Systems, IEEE Transactions on*, vol. 27, no. 2, pp. 922–931, May 2012.

[8] T. Franch, M. Scheidt, and G. Stock, "Current and future challenges for production planning systems," in *Optimization in the Energy Industry*, ser. Energy Systems, J. Kallrath, P. Pardalos, S. Rebennack, and M. Scheidt, Eds. Springer Berlin Heidelberg, 2009, pp. 5–17.

[9] J. Carpentier, "Contribution to the economic dispatch problem," *Bulletin Society Francaise Electriciens*, vol. 23, no. 8, pp. 431–447, 1962.

[10] P. Biskas, N. Ziogos, A. Tellidou, C. Zoumas, A. Bakirtzis, and V. Petridis, "Comparison of two metaheuristics with mathematical programming methods for the solution of opf," *Generation, Transmission and Distribution, IEE Proceedings*, vol. 153, no. 1, pp. 16–24, Jan 2006.

[11] W. B. Wood, A., "Power generation operation and control," *Wiley, New York*, 1996.

[12] N. Rau, "Issues in the path toward an rto and standard markets," *Power Systems, IEEE Transactions on*, vol. 18, no. 2, pp. 435–443, May 2003.

[13] A. Azmy, "Optimal power flow to manage voltage profiles in interconnected networks using expert systems," *Power Systems, IEEE Transactions on*, vol. 22, no. 4, pp. 1622–1628, Nov 2007.

[14] B. Chowdhury and S. Rahman, "A review of recent advances in economic dispatch," *Power Systems, IEEE Transactions on*, vol. 5, no. 4, pp. 1248–1259, Nov 1990.

[15] M. Huneault and F. Galiana, "A survey of the optimal power flow literature," *Power Systems, IEEE Transactions on*, vol. 6, no. 2, pp. 762–770, May 1991.

[16] J. Momoh, R. Adapa, and M. El-Hawary, "A review of selected optimal power flow literature to 1993. i. nonlinear and quadratic programming approaches," *Power Systems, IEEE Transactions on*, vol. 14, no. 1, pp. 96–104, Feb 1999.

[17] J. Momoh, M. El-Hawary, and R. Adapa, "A review of selected optimal power flow literature to 1993. ii. newton, linear programming and interior point methods," *Power Systems, IEEE Transactions on*, vol. 14, no. 1, pp. 105–111, Feb 1999.

[18] Y. Xiao, Y. H. Song, and Y.-Z. Sun, "Power flow control approach to power systems with embedded facts devices," *Power Systems, IEEE Transactions on*, vol. 17, no. 4, pp. 943–950, Nov 2002.

[19] R. Jabr, "Optimal power flow using an extended conic quadratic formulation," *Power Systems, IEEE Transactions on*, vol. 23, no. 3, pp. 1000–1008, 2008.

[20] M. Baradar, M. Hesamzadeh, and M. Ghandhari, "Modelling of multi-terminal hvdc systems in optimal power flow formulation," in *Electrical Power and Energy Conference (EPEC), 2012 IEEE*, Oct 2012, pp. 170–175.

[21] K. Almeida and F. Galiana, "Critical cases in the optimal power flow," *Power Systems, IEEE Transactions on*, vol. 11, no. 3, pp. 1509–1518, Aug 1996.

[22] W.-M. Lin, C.-H. Huang, and T.-S. Zhan, "A hybrid current-power optimal power flow technique," *Power Systems, IEEE Transactions on*, vol. 23, no. 1, pp. 177–185, Feb 2008.

[23] N. Rau, "Optimization principles: Practical applications to the operation and markets of the electric power industry," *Wiley/IEEE Press, Hoboken*, 2003.

[24] B. Stott, J. Jardim, and O. Alsac, "Dc power flow revisited," *Power Systems, IEEE Transactions on*, vol. 24, no. 3, pp. 1290–1300, Aug 2009.

[25] J. Das, "Power system analysis: Short-circuit load flow and harmonics," *CRC Press, Boca Raton*, 2002.

[26] J. Momoh, R. Koessler, M. Bond, B. Stott, D. Sun, A. Papalexopoulos, and P. Ristanovic, "Challenges to optimal power flow," *Power Systems, IEEE Transactions on*, vol. 12, no. 1, pp. 444–455, Feb 1997.

[27] P. P. T. N. Horst, R., "Introduction to global optimization," *2nd edn. Springer, Berlin*, 2000.

[28] S. Tripathy, G. Prasad, O. P. Malik, and G. Hope, "Load-flow solutions for ill-conditioned power systems by a newton-like method," *Power Apparatus and Systems, IEEE Transactions on*, vol. PAS-101, no. 10, pp. 3648–3657, 1982.

[29] M. Haque, "A general load flow method for distribution systems," *Electric Power Systems Research*, vol. 54, no. 1, pp. 47 – 54, 2000.

[30] W. H. Kersting, *Distribution System Modeling and Analysis*. Boca Raton, FL: CRC, 2012.

[31] M. F. AlHajri and M. El-Hawary, "Exploiting the radial distribution structure in developing a fast and flexible radial power flow for unbalanced three-phase networks," *Power Delivery, IEEE Transactions on*, vol. 25, no. 1, pp. 378–389, 2010.

[32] G. Chang, S.-Y. Chu, M.-F. Hsu, C.-S. Chuang, and H.-L. Wang, "An efficient power flow algorithm for weakly meshed distribution systems," *Electric Power Systems Research*, vol. 84, no. 1, pp. 90 – 99, 2012.

[33] J.-H. Teng, "A direct approach for distribution system load flow solutions," *Power Delivery, IEEE Transactions on*, vol. 18, no. 3, pp. 882–887, 2003.

[34] R. Jabr, "Radial distribution load flow using conic programming," *Power Systems, IEEE Transactions on*, vol. 21, no. 3, pp. 1458–1459, 2006.

[35] F. Alizadeh and D. Goldfarb, "Second-order cone programming," *Mathematical Programming (Series B)*, vol. 95, no. 1, pp. 3–51, 2003. [Online]. Available: http://rutcor.rutgers.edu/ alizadeh/CLASSES/03sprNLP/Papers/allSurvey.pdf

[36] M. S. Lobo, L. Vandenberghe, S. Boyd, and H. Lebret, "Applications of second-order cone programming," *Linear Algebra and its Applications*, vol. 284, no. 1-3, pp. 193 – 228, 1998.

[37] M. R. Irving and M. J. H. Sterling, *International Journal of Electrical Power and Energy Systems.*

[38] C. R. E. D. Andersen and T. Terlaky, "On implementing a primal-dual interior-point method for conic quadratic optimization," 2000. [Online]. Available: http:www.optimization-online.org/DB-FILE/2000/12/245.pdf

[39] "Gams/mosek." [Online]. Available: http:www.gams.com/dd/docs/solvers/mosek.pdf

[40] D. Das, H. S. Nagi, and D. Kothari, "Novel method for solving radial distribution networks," *Generation, Transmission and Distribution, IEE Proceedings-*, vol. 141, no. 4, pp. 291–298, 1994.

[41] D. Das, D. Kothari, and A. Kalam, "Simple and efficient method for load flow solution of radial distribution networks," *International Journal of Electrical Power and Energy Systems*, vol. 17, no. 5, pp. 335 – 346, 1995.

[42] R. RANJAN and DAS, "Simple and efficient computer algorithm to solve radial distribution networks," *Electric Power Components and Systems*, vol. 31, no. 1, pp. 95–107, 2003.

[43] D. Molzahn and B. Lesieutre, "Initializing dynamic power system simulations using eigenvalue formulations of the induction machine and power flow models," *Circuits and Systems I: Regular Papers, IEEE Transactions on*, vol. 60, no. 3, pp. 690–702, 2013.

[44] J. Glover, M. Sarma, and T. Overbye, "Power system analysis and design," *Lubbock, TX. CL Engineering*, 2011.

[45] B. Stott, "Review of load-flow calculation methods," *Proceedings of the IEEE*, vol. 62, no. 7, pp. 916–929, July 1974.

[46] Y. Kumar, K. Dwivedi, and G. Agnihotri, "Development of ant algorithm for load flow analysis," in *Power Systems Conference and Exposition, 2009. PSCE '09. IEEE/PES*, 2009, pp. 1–5.

[47] K. Wong, A. Li, and M. Law, "Development of constrained-genetic-algorithm load-flow method," *Generation, Transmission and Distribution, IEE Proceedings-*, vol. 144, no. 2, pp. 91–99, 1997.

[48] W. F. Tinney and C. Hart, "Power flow solution by newton's method," *Power Apparatus and Systems, IEEE Transactions on*, vol. PAS-86, no. 11, pp. 1449–1460, 1967.

[49] V. da Costa, N. Martins, and J. L. R. Pereira, "Developments in the newton raphson power flow formulation based on current injections," *Power Systems, IEEE Transactions on*, vol. 14, no. 4, pp. 1320–1326, 1999.

[50] A. Exposito and E. Ramos, "Augmented rectangular load flow model," *Power Systems, IEEE Transactions on*, vol. 17, no. 2, pp. 271–276, 2002.

[51] R. Jabr, "A conic quadratic format for the load flow equations of meshed networks," *Power Systems, IEEE Transactions on*, vol. 22, no. 4, pp. 2285–2286, 2007.

[52] M. Farivar and S. Low, "Branch flow model: Relaxations and convexification," in *Decision and Control (CDC), 2012 IEEE 51st Annual Conference on*, 2012, pp. 3672–3679.

[53] J. Taylor and F. Hover, "Conic ac transmission system planning," *Power Systems, IEEE Transactions on*, vol. 28, no. 2, pp. 952–959, 2013.

[54] M. Baradar and M. Hesamzadeh, "Ac power flow representation in conic format," *Power Systems, IEEE Transactions on*, vol. 30, no. 1, pp. 546–547, Jan 2015.

[55] J. J. Grainger and W. D. Stevenson, *Power System Analysis*. McGraw-Hill, 1994.

[56] *The University of Washington Power Systems Test Case Archive*. [On-line]. Available: http://www.ee.washington.edu/research/pstca/.

[57] X. Bai, H. Wei, K. Fujisawa, and Y. Wang, "Semidefinite programming for optimal power flow problems," *International Journal of Electrical Power and Energy Systems*, vol. 6-7, pp. 383–392, 2008.

[58] J. Lavaei and S. Low, "Zero duality gap in optimal power flow problem," *Power Systems, IEEE Transactions on*, vol. 27, no. 1, pp. 92 –107, feb. 2012.

[59] M. Baradar and M. Hesamzadeh, "Calculating negative lmps from socp-opf," in *Energy Conference (ENERGYCON), 2014 IEEE International*, May 2014, pp. 1461–1466.

[60] F. Genoese, M. Genoese, and M. Wietschel, "Occurrence of negative prices on the german spot market for electricity and their influence on balancing power markets," in *Energy Market (EEM), 2010 7th International Conference on the European*, June 2010, pp. 1–6.

[61] "European energy exchange, "eex customer information: Important notes with regard to changeover of day ahead power trading on september 1, 2008," 28/08/2008." [Online]. Available: http://www.eex.com/de

[62] B. Hobbs, G. Drayton, E. Fisher, and W. Lise, "Improved transmission representations in oligopolistic market models: Quadratic losses, phase shifters, and dc lines," *Power Systems, IEEE Transactions on*, vol. 23, no. 3, pp. 1018–1029, 2008.

[63] A. J. Wood and B. F. Wollenbergy, *Power Generation, Operation, and Control*. New York: Wiley, 1984.

[64] H. Zhong, Q. Xia, Y. Wang, and C. Kang, "Dynamic economic dispatch considering transmission losses using quadratically constrained quadratic program method," *Power Systems, IEEE Transactions on*, vol. 28, no. 3, pp. 2232–2241, 2013.

[65] O. Akinbode and K. Hedman, "Fictitious losses in the dcopf with a piecewise linear approximation of losses," in *Power and Energy Society General Meeting (PES), 2013 IEEE*, 2013, pp. 1–5.

[66] H. Zhang, V. Vittal, G. Heydt, and J. Quintero, "A mixed-integer linear programming approach for multi-stage security-constrained transmission expansion planning," *Power Systems, IEEE Transactions on*, vol. 27, no. 2, pp. 1125–1133, 2012.

[67] R. Zimmerman, C. Murillo-Sandnchez, and R. Thomas, "MATPOWER: Steady-state operations, planning, and analysis tools for power systems research and education," *Power Systems, IEEE Transactions on*, vol. 26, no. 1, pp. 12 –19, feb. 2011.

[68] S. Massoud Amin and B. Wollenberg, "Toward a smart grid: power delivery for the 21st century," *Power and Energy Magazine, IEEE*, vol. 3, no. 5, pp. 34 – 41, sept.-oct. 2005.

[69] D. Van Hertem, J. Rimez, and R. Belmans, "Power flow controlling devices as a smart and independent grid investment for flexible grid operations: Belgian case study," *Smart Grid, IEEE Transactions on*, vol. 4, no. 3, pp. 1656–1664, 2013.

[70] M. Claus, D. Retzmann, D. Sorangr, and K. Uecker, "Solutions for Smart and Super Grids with HVDC and FACTS, Technical article Published by Siemens AG," *[Online]. Available: http://www.ptd.siemens.de/CEPSI08_Art.pdf*, October 2008.

[71] M. Baradar, M. Ghandhari, and D. Van Hertem, "The modeling multi-terminal vsc-hvdc in power flow calculation using unified methodology," in *Innovative Smart Grid Technologies (ISGT Europe), 2011 2nd IEEE PES International Conference and Exhibition on*, Dec 2011, pp. 1–6.

[72] M. Baradar, M. Ghandhari, D. Van Hertem, and A. Kargarian, "Power flow calculation of hybrid ac/dc power systems," in *Power and Energy Society General Meeting, 2012 IEEE*, July 2012, pp. 1–6.

[73] A. Pizano-Martinez, C. Fuerte-Esquivel, H. Ambriz-Perez, and E. Acha, "Modeling of VSC-Based HVDC systems for a Newton-Raphson OPF algorithm," *Power Systems, IEEE Transactions on*, vol. 22, no. 4, pp. 1794 –1803, nov. 2007.

[74] H. Ambriz-Perez, E. Acha, and C. Fuerte-Esquivel, "Advanced svc models for newton-raphson load flow and newton optimal power flow studies," *Power Systems, IEEE Transactions on*, vol. 15, no. 1, pp. 129–136, 2000.

[75] X. Wei, J. Chow, B. Fardanesh, and A.-A. Edris, "A common modeling framework of voltage-sourced converters for load flow, sensitivity, and dispatch analysis," *Power Systems, IEEE Transactions on*, vol. 19, no. 2, pp. 934 – 941, may 2004.

[76] M. Baradar and M. Ghandhari, "A multi-option unified power flow approach for hybrid ac/dc grids incorporating multi-terminal vsc-hvdc," *Power Systems, IEEE Transactions on*, vol. 28, no. 3, pp. 2376–2383, Aug 2013.

[77] M. Baradar, "Modeling of multi terminal hvdc systemsin power flow and optimal power flow formulations," *Licentiate thesis, KTH Royal Institute of Technology*, January 2013.

[78] E. Santacana, T. Zucco, X. Feng, J. Pan, M. Mousavi, and L. Tang, "Power to be efficient, ABB Review 2," *[Online]. Available: http://www05.abb.com*, 2007.

[79] "Energy Information Administration," *[Online]. Available: www.eia.doe.gov*.

[80] J. Ramos, A. Exposito, and V. Quintana, "Transmission power loss reduction by interior-point methods: implementation issues and practical experience," *Generation, Transmission and Distribution, IEE Proceedings-*, vol. 152, no. 1, pp. 90 –98, jan. 2005.

[81] V. de Sousa, E. Baptista, and G. da Costa, "Loss minimization by the predictor-corrector modified barrier approach," *Electric Power Systems Research*, vol. 79, no. 5, pp. 803 – 808, 2009.

[82] M. Tripathy and S. Mishra, "Bacteria Foraging-Based Solution to Optimize Both Real Power Loss and Voltage Stability Limit," *Power Systems, IEEE Transactions on*, vol. 22, no. 1, pp. 240 –248, Feb. 2007.

[83] P. Roy, S. P. Ghoshal, and S. S. Thakur, "Optimal VAR control for improvements in voltage profiles and for real power loss minimization using Biogeography Based Optimization," *International Journal of Electrical Power & Energy Systems*, vol. 43, no. 1, pp. 830 – 838, may 2012.

[84] G. Daelemans, K. Srivastava, M. Reza, S. Cole, and R. Belmans, "Minimization of steady-state losses in meshed networks using vsc hvdc," in *Power Energy Society General Meeting, 2009. PES '09. IEEE*, july 2009, pp. 1 –5.

[85] J. Zhu, K. Cheung, D. Hwang, and A. Sadjadpour, "Operation Strategy for Improving Voltage Profile and Reducing System Loss," *Power Delivery, IEEE Transactions on*, vol. 25, no. 1, pp. 390 –397, jan. 2010.

[86] D. Thukaram and G. Yesuratnam, "Optimal reactive power dispatch in a large power system with AC-DC and FACTS controllers," *Generation, Transmission Distribution, IET*, vol. 2, no. 1, pp. 71 –81, january 2008.

[87] P. Preedavichit and S. Srivastava, "Optimal reactive power dispatch considering FACTS devices," *Electric Power Systems Research*, vol. 46, no. 3, pp. 251 – 257, 1998.

[88] J. Cao, W. Du, H. Wang, and S. Bu, "Minimization of transmission loss in meshed ac/dc grids with vsc-mtdc networks," *Power Systems, IEEE Transactions on*, vol. 28, no. 3, pp. 3047–3055, 2013.

[89] B. Han, G. Karady, J. Park, and S. Moon, "Interaction analysis model for transmission static compensator with emtp," *Power Delivery, IEEE Transactions on*, vol. 13, no. 4, pp. 1297–1302, 1998.

[90] "Ensuring green growth in a time of economic crisis, the role of energy technology," *International Energy Agency, Siracusa, Italy.*, 2009.

[91] "A breath of fresh air, ewea 2009 annual report." *European Wind Energy Association.*, April 2010. [Online]. Available: http://www.ewea.org/fileadmin/ewea documents/documents/ publications/reports/Ewea Annual Report 2009.pdf

[92] "Pure power - wind energy scenarios up to 2030," *European Wind Energy Association.*, March 2008. [Online]. Available: http://www.ewea.org/fileadmin/ewea documents/documents/ publications/reports/purepower.pdf

[93] "Analysis of dynamic behavior of electric power systems with large amount of wind power," *Ph.D. dissertation, Technical Univ. Denmark, Lyngby, Denmark*, 2003.

[94] A. Feijoo and J. Cidras, "Modeling of wind farms in the load flow analysis," *Power Systems, IEEE Transactions on*, vol. 15, no. 1, pp. 110–115, Feb 2000.

[95] A. Keane, P. Cuffe, E. Diskin, D. Brooks, P. Harrington, T. Hearne, M. Rylander, and T. Fallon, "Evaluation of advanced operation and control of distributed wind farms to support efficiency and reliability," *Sustainable Energy, IEEE Transactions on*, vol. 3, no. 4, pp. 735–742, Oct 2012.

[96] L.-R. Chang-Chien and Y.-C. Yin, "Strategies for operating wind power in a similar manner of conventional power plant," *Energy Conversion, IEEE Transactions on*, vol. 24, no. 4, pp. 926–934, Dec 2009.

[97] K. Zou, A. Agalgaonkar, K. Muttaqi, and S. Perera, "Distribution system planning with incorporating dg reactive capability and system uncertainties," *Sustainable Energy, IEEE Transactions on*, vol. 3, no. 1, pp. 112–123, Jan 2012.

[98] E. Vittal, M. O'Malley, and A. Keane, "Rotor angle stability with high penetrations of wind generation," *Power Systems, IEEE Transactions on*, vol. 27, no. 1, pp. 353–362, Feb 2012.

[99] J. Hu and Y. He, "Reinforced control and operation of dfig-based wind-power-generation system under unbalanced grid voltage conditions," *Energy Conversion, IEEE Transactions on*, vol. 24, no. 4, pp. 905–915, Dec 2009.

[100] M. Martinez, G. Tapia, A. Susperregui, and H. Camblong, "Dfig power generation capability and feasibility regions under unbalanced grid voltage conditions," *Energy Conversion, IEEE Transactions on*, vol. 26, no. 4, pp. 1051–1062, Dec 2011.

[101] C. Chompoo-inwai, C. Yingvivatanapong, K. Methaprayoon, and W.-J. Lee, "Reactive compensation techniques to improve the ride-through capability of wind turbine during disturbance," *Industry Applications, IEEE Transactions on*, vol. 41, no. 3, pp. 666–672, May 2005.

[102] "Wind and solar curtailment," *National Renewable Energy Laboratory (NREL)*. [Online]. Available: http://www.nrel.gov/publications

[103] A. Tamimi, A. Pahwa, and S. Starrett, "Method for assessing system impact of increasing wind farm sizes above their maximum limits," in *Power and Energy Society General Meeting, 2011 IEEE*, July 2011, pp. 1–8.

[104] B. Gao, G. Morison, and P. Kundur, "Voltage stability evaluation using modal analysis," *Power Systems, IEEE Transactions on*, vol. 7, no. 4, pp. 1529–1542, Nov 1992.

[105] N. T. Linh, "Voltage stability analysis of grids connected wind generators," in *Industrial Electronics and Applications, 2009. ICIEA 2009. 4th IEEE Conference on*, May 2009, pp. 2657–2660.

[106] M. Chinchilla, S. Arnalte, J. Burgos, and J. Rodríguez, "Power limits of grid-connected modern wind energy systems," *Renewable Energy*, vol. 31, no. 9, pp. 1455 – 1470, 2006.

[107] A. Tamimi, A. Pahwa, S. Starrett, and N. Williams, "Maximizing wind penetration using voltage stability based methods for sizing and locating new wind farms in power system," in *Power and Energy Society General Meeting, 2010 IEEE*, July 2010, pp. 1–7.

[108] A. Tamimi, A. Pahwa, and S. Starrett, "Effective wind farm sizing method for weak power systems using critical modes of voltage instability," *Power Systems, IEEE Transactions on*, vol. 27, no. 3, pp. 1610–1617, Aug 2012.

[109] A. Keane, L. Ochoa, E. Vittal, C. Dent, and G. Harrison, "Enhanced utilization of voltage control resources with distributed generation," *Power Systems, IEEE Transactions on*, vol. 26, no. 1, pp. 252–260, Feb 2011.

[110] E. Vittal, A. Keane, and M. O'Malley, "Varying penetration ratios of wind turbine technologies for voltage and frequency stability," in *Power and Energy Society General Meeting - Conversion and Delivery of Electrical Energy in the 21st Century, 2008 IEEE*, July 2008, pp. 1–6.

[111] E. Vittal, M. O'Malley, and A. Keane, "A steady-state voltage stability analysis of power systems with high penetrations of wind," *Power Systems, IEEE Transactions on*, vol. 25, no. 1, pp. 433–442, Feb 2010.

[112] V. Kumar, K. Reddy, and D. Thukaram, "Coordination of reactive power in grid-connected wind farms for voltage stability enhancement," *Power Systems, IEEE Transactions on*, vol. 29, no. 5, pp. 2381–2390, Sept 2014.

[113] A. Almeida, E. Valenca de Lorenci, R. Coradi Leme, A. Zambroni de Souza, B. Lima Lopes, and K. Lo, "Probabilistic voltage stability assessment considering renewable sources with the help of the pv and qv curves," *Renewable Power Generation, IET*, vol. 7, no. 5, pp. 521–530, Sept 2013.

[114] E. Haesen, C. Bastiaensen, J. Driesen, and R. Belmans, "A probabilistic formulation of load margins in power systems with stochastic generation," *Power Systems, IEEE Transactions on*, vol. 24, no. 2, pp. 951–958, May 2009.

[115] L. Xu, L. Yao, and C. Sasse, "Grid integration of large dfig-based wind farms using vsc transmission," *Power Systems, IEEE Transactions on*, vol. 22, no. 3, pp. 976–984, Aug 2007.

[116] D. W. E. Eriksson, P. Halvarsson and M. Hausler, "System approach on designing an offshore wind power grid connection," *4th Int. Workshop Large-Scale Integration of Wind Power and Transmission Networks for Offshore Wind Farms*, 2003.

[117] S. M. Bolik, "System approach on designing an offshore wind power grid connection," *4th Int. Workshop Large-Scale Integration of Wind Power and Transmission Networks for Offshore Wind Farms*, 2003.

[118] X. Koutiva, T. Vrionis, N. Vovos, and G. Giannakopoulos, "Optimal integration of an offshore wind farm to a weak ac grid," *Power Delivery, IEEE Transactions on*, vol. 21, no. 2, pp. 987–994, April 2006.

[119] L. Xu and B. R. Andersen, "Grid connection of large offshore wind farms using hvdc," *Wind Energy*, vol. 9, no. 4, pp. 371–382, 2006.

[120] W. Lu and B.-T. Ooi, "Optimal acquisition and aggregation of offshore wind power by multiterminal voltage-source hvdc," *Power Delivery, IEEE Transactions on*, vol. 18, no. 1, pp. 201–206, Jan 2003.

[121] "Delivering a secure sustainable electricity system," *EirGrid and SONI*, 2013.

[122] A. Conejo, F. Milano, and R. Garcia-Bertrand, "Congestion management ensuring voltage stability," *Power Systems, IEEE Transactions on*, vol. 21, no. 1, pp. 357–364, Feb 2006.

[123] M. Lei, L. Shiyan, J. Chuanwen, L. Hongling, and Z. Yan, "A review on the forecasting of wind speed and generated power," *Renewable and Sustainable Energy Reviews*, vol. 13, no. 4, pp. 915 – 920, 2009.

[124] J. Matevosyan and L. Soder, "Minimization of imbalance cost trading wind power on the short-term power market," *Power Systems, IEEE Transactions on*, vol. 21, no. 3, pp. 1396–1404, 2006.

[125] H. Heitsch and W. Romisch, "Scenario reduction algorithms in stochastic programming," *Computational Optimization and Applications*, vol. 24, no. 2-3, pp. 187–206, 2003.

[126] J. Dupacova, G. Consigli, and S. Wallace, "Scenarios for multistage stochastic programs," *Annals of Operations Research*, vol. 100, no. 1-4, pp. 25–53, 2000.

[127] G. Boyle, *Renewable energy*, O. U. Press, Ed. Oxford University Press, 2004.

[128] S. Roy, "Market constrained optimal planning for wind energy conversion systems over multiple installation sites," *Energy Conversion, IEEE Transactions on*, vol. 17, no. 1, pp. 124–129, 2002.

Part V

Publications